CHAPTER 4

Dysprosium Acylpyrazolone complexes: Synthesis, Structural Features, Fluorescence and Electronic properties.

4.1 Introduction

The fluorescence characteristics of lanthanide acylpyrazolone derivatives have drawn more interest in recent years to the topic of coordination chemistry [1]. Complexes of coumarin analogues of lanthanide ions were shown to have beneficial biological and pharmaceutical properties [2]. Complexes of pyrazoline and pyridine analogues of lanthanides are known for luminescent, optical, magnetic and metamaterial behaviour [3–5]. An ionic derivative of acylpyrazolones ($Me_3NC_{16}H_{33}$) [$Al(Q_4Q)_2$], first revealed their fluorescence activity [6]. Most frequently, low-intensity fluorescence and phosphorescence spectra were seen in terbium and europium complexes with the general formula [$M(Q)_3(H_2O)_2$], [$M(Q)_3(EtOH)$], or [$M(Q)_4$], which have been associated to the auxiliary donors and substituents in acylpyrazolone ligands [7–9]. This suggests the potential application of these complexes in the fabrication of display devices. In the ($Me_3NC_{16}H_{33}$)[$Ln(Q_3Q)_2$] system, particularly with Sm^{3+}, Lu^{3+}, Y^{3+}, Gd^{3+} and Tb^{3+}, a good fluorescence enhancement effect with high intensity has been reported [1]. The approach for identifying nucleic acids is improved by the fluorescence quenching caused by nucleic acid in such a system [10]. In their 2022 study, Jiang and colleagues explored the impact of steric hindrance from Schiff-base ligands on the magnetic relaxation dynamics and emissive properties of two dinuclear dysprosium complexes [11]. Hooda and their research team synthesized Dy(III) complexes exhibiting yellow luminescence, showcasing their potential for developing high-efficiency organic light-emitting materials [12]. These complexes possess desirable properties such as a suitable band gap, excellent thermal stability, and remarkable luminous characteristics, making them promising candidates for the fabrication of OLEDs and displays. Dalal and colleagues' research team has documented improvements in the photophysical properties of octacoordinated Dy(III) complexes through energy transfer facilitated by photosensitizing ligands [13]. The series of octa-coordinated Dy(III) complexes, as described in Redhu et al.'s publication, exhibit yellow emission when paired with 1,3-diphenylprop-1,3-dione (DPD) and bidentate N donor neutral ligands [14]. Most lanthanide ions can display fluorescence, in which Dy^{3+} possesses distinctive properties due to its increased intensity, composition and symmetry of the coordination sphere, illuminating their favoured application [15].

Fluorescence and luminescence activity in Dysprosium complexes is primarily determined by factors such as low synthesis costs, strong chemical-thermal stability, proper host or ligand selection, yellow-to-blue emission intensity ratio, etc [16]. White light emission mechanism of Dysprosium materials makes it easier to employ them in WLEDs and other high-tech solid-state lighting systems [17]. In the current Chapter, six Dysprosium-acylpyrazolone complexes were synthesized and characterized. The main objective is to analyze their covalency and fluorescence to create a quick, easy, and accurate approach for detecting minute levels of Dy^{3+}.

4.2 Experimental section

4.2.1 Materials and Methods

All six ligands **[**((4-chlorophenyl)(5-hydroxy-3-methyl 1-(phenyl = **HL^1** / 3-chlorophenyl = **HL^2** / p-tolyl = **HL^3**) -1H-pyrazol-4-yl)methanone), (3,5-dimethyl phenyl)(5-hydroxy 1-(phenyl = **HL^4** / 3-chlorophenyl = **HL^5** / p-tolyl = **HL^6**) -1H-pyrazol-4-yl)methanone**]** were directly prepared and used exactly as we described in Chapter 2(a). 99.9% extrapure Dysprosium(III) nitrate hexahydrate was purchased from Chemdyes Corporation. Dysprosium nitrate was stored in a closed container in a dry place as it is moisture sensitive, and it was taken in the experiment using a spatula after wearing protective gloves.

4.2.2 Synthesis of Dysprosium-acylpyrazolone complexes

A 1:1 ethanolic combination of 3 eq ethanolic solution of ligand and 3 eq $NaOH_{(aq)}$ was stirred in the combined assembly of the round bottom flask and water condenser at room atmosphere for a half-hour at 80–100 °C as shown in Figure 4.1. Then, 1 eq ethanolic solution of Dysprosium(III) nitrate hexahydrate was added in a dropwise manner. After 18 hours of refluxing, the solution was transferred to a container where it was slowly evaporated to produce an eight-coordinated Dysprosium-acylpyrazolone complex. Refluxing a mixture aims to speed up and induce the reaction occurring. After the solvent has gradually evaporated, the complex product will precipitate. The unreacted ligand and Dysprosium(III) nitrate will remain in the supernatant.

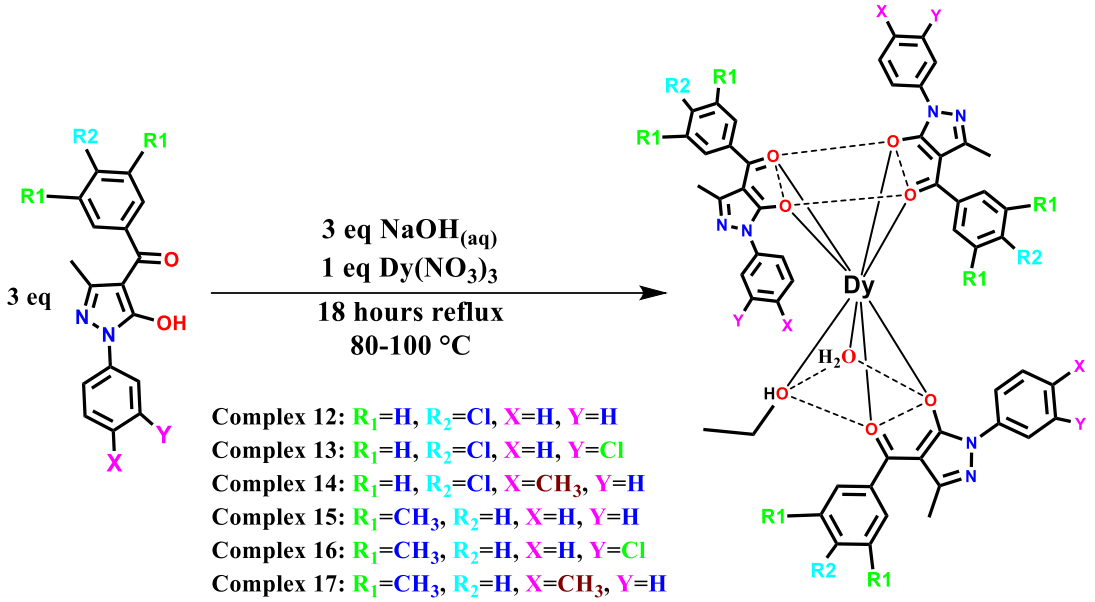

Figure 4.1 Synthetic route for Dysprosium-acylpyrazolone complexes.

Complex 12 Synthesis

$[Dy(L^1)_3(EtOH)(H_2O)]$ (complex 12) was prepared using 3 eq HL^1 ligand (3 mmol, 0.9375 g), 3 eq $NaOH_{(aq)}$ (3 mmol, 0.12 g), and 1 eq Dysprosium(III) nitrate (1 mmol, 0.348 g). Yield (%): 91%, M.P.: >200 °C, Molecular formula: $C_{53}H_{44}Cl_3N_6DyO_8$, Formula wt: 1161.82. **FTIR (KBr, cm^{-1}):** 3063 (w, $\upsilon_{O\text{-}H\ water}$), 2926 (w, $\upsilon_{O\text{-}H\ EtOH}$), 1612 (s, $\upsilon_{C=O\ PCB}$), 1592 (s, $\upsilon_{C=O\ acylpyz}$).

Complex 13 Synthesis

$[Dy(L^2)_3(EtOH)(H_2O)]$ (complex 13) was prepared using 3 eq HL^2 ligand (3 mmol, 1.0416 g), 3 eq $NaOH_{(aq)}$ (3 mmol, 0.12 g), and 1 eq Dysprosium(III) nitrate (1 mmol, 0.348 g). Yield (%): 86%, M.P.: >200 °C, Molecular formula: $C_{53}H_{41}Cl_6N_6DyO_8$, Formula wt: 1263.04. **FTIR (KBr, cm^{-1}):** 3105 (w, $\upsilon_{O\text{-}H\ water}$), 2972 (w, $\upsilon_{O\text{-}H\ EtOH}$), 1613 (s, $\upsilon_{C=O\ PCB}$), 1589 (s, $\upsilon_{C=O\ acylpyz}$).

Complex 14 Synthesis

$[Dy(L^3)_3(EtOH)(H_2O)]$ (complex 14) was prepared using 3 eq HL^3 ligand (3 mmol, 0.9795 g), 3 eq $NaOH_{(aq)}$ (3 mmol, 0.12 g), and 1 eq Dysprosium(III) nitrate (1 mmol, 0.348 g). Yield (%): 91%, M.P.: >200 °C, Molecular formula: $C_{56}H_{50}Cl_3N_6DyO_8$, Formula wt: 1203.20. **FTIR (KBr, cm^{-1}):** 3034 (w, $\upsilon_{O\text{-}H\ water}$), 2926 (w, $\upsilon_{O\text{-}H\ EtOH}$), 1601 (s, $\upsilon_{C=O\ PCB}$), 1504 (s, $\upsilon_{C=O\ acylpyz}$).

Complex 15 Synthesis

$[Dy(L^4)_3(EtOH)(H_2O)]$ (complex 15) was prepared using 3 eq HL^4 ligand (3 mmol, 0.92 g), 3 eq $NaOH_{(aq)}$ (3 mmol, 0.12 g), and 1 eq Dysprosium(III) nitrate (1 mmol, 0.348 g). The bright yellow plate-type crystals of complex 15 were obtained through recrystallization in DMF and slow evaporation technique. Yield(%): 87%, M.P.: >200 °C, Molecular formula: $C_{59}H_{59}N_6DyO_8$, Formula wt: 1142.66. **FTIR (KBr, cm^{-1}):** 3408 (w, $\upsilon_{O\text{-}H\ water}$), 2923 (w, $\upsilon_{O\text{-}H\ EtOH}$), 1613 (s, $\upsilon_{C=O\ DMB}$), 1581 (s, $\upsilon_{C=O\ acylpyz}$).

Complex 16 Synthesis

$[Dy(L^5)_3(EtOH)(H_2O)]$ (complex 16) was prepared using 3 eq HL^5 ligand (3 mmol, 1.023 g), 3 eq $NaOH_{(aq)}$ (3 mmol, 0.12 g), and 1 eq Dysprosium(III) nitrate (1 mmol, 0.348 g). Yield(%): 81%, M.P.: >200 °C, Molecular formula: $C_{59}H_{56}Cl_3N_6DyO_8$, Formula wt: 1245.25. **FTIR (KBr, cm^{-1}):** 3109 (w, $\upsilon_{O\text{-}H\ water}$), 2921 (w, $\upsilon_{O\text{-}H\ EtOH}$), 1615 (s, $\upsilon_{C=O\ DMB}$), 1588 (s, $\upsilon_{C=O\ acylpyz}$).

Complex 17 Synthesis

$[Dy(L^6)_3(EtOH)(H_2O)]$ (complex 17) was prepared using 3 eq HL^6 ligand (3 mmol, 0.96 g), 3 eq $NaOH_{(aq)}$ (3 mmol, 0.12 g), and 1 eq Dysprosium(III) nitrate (1 mmol, 0.348 g). Yield(%): 88%, M.P.: >200 °C, Molecular formula: $C_{62}H_{65}N_6DyO_8$, Formula wt: 1184.74. **FTIR (KBr, cm^{-1}):** 3034 (w, $\upsilon_{O\text{-}H\ water}$), 2921 (w, $\upsilon_{O\text{-}H\ EtOH}$), 1619 (s, $\upsilon_{C=O\ DMB}$), 1597 (s, $\upsilon_{C=O\ acylpyz}$).

4.2.3 Physical measurements and characterization techniques

Similar techniques, software, or equipment were employed to assess the data of synthesized compounds obtained through FTIR, mass, UV-Vis, and TG-DTA, as provided in Chapter 3(a). Solid-state emission spectra were recorded using a Jasco FP-6300 spectrofluorometer by taking powders on a glass slide. The single crystal X-ray data was collected on a Bruker D8 Quest CCD device with graphite monochromator and Mo-Kα radiation (λ = 0.71073 Å). The SHELXT and SHELXL-2019/2 software were used to solve the diffraction data and perform the computation [18,19]. Powder XRD measurements were done on the SmartLab SE (3kW) model of Rigaku, Japan, using SmartLab Studio II software and a Cu-Kα (0.154 nm) source with D/teX Ultra 250 1D detector was used.

4.3 Results and Discussion

For the complexes 12, 13, 14, 15, 16, and 17, the molar conductivity Λ_M values were found to be 9.8, 7.03, 6.87, 4.83, 5.74 and 8.64 Ω^{-1} cm^2 mol^{-1}, respectively in DMF solvent. These lower numbers demonstrate the non-electrolytic behaviour [20]. Moreover, the mass, FTIR, TG-DTA, powder and single crystal X-ray data of the Dysprosium acylpyrazolone complexes have been analyzed to study their geometry confirmation, covalent qualities, and other spectral aspects as shown in the following sections.

4.3.1 Mass spectrometric analysis

Mass spectra of complexes 12, 13, 16, and 17 were recorded in methanol/acetonitrile solvent, and its compatibility with the suggested geometry is discussed. The complexes 12, 13, 16, and 17 show m/z peak of protonated ligand ([H-L]$^+$) peak at 313.06 ($[C_{17}H_{13}ClN_2O_2]^+$), 347.02 ($[C_{17}H_{12}Cl_2N_2O_2]^+$), 341.12 ($[C_{19}H_{17}ClN_2O_2]^+$), and 321.17 ($[C_{20}H_{20}N_2O_2]^+$), respectively. As all mass spectra were recorded in methanol/acetonitrile solvent, the replacement of ethanol and water from the suggested geometry $[Dy(L)_3(EtOH)(H_2O)]$ by methanol and acetonitrile is observed. Therefore, corresponding m/z peaks for geometry $[Dy(L)_3(MeOH)(CH_3CN)]$ are observed at around 1172.09 ($[C_{54}H_{43}Cl_3N_7DyO_7]^+$) in complex 12, 1272.05 ($[C_{54}H_{40}Cl_6N_7DyO_7]^+$) in complex 13, 1256.27 ($[C_{60}H_{55}Cl_3N_7DyO_7]^+$) in complex 16, and 1194.43 ($[C_{63}H_{64}N_7DyO_7]^+$) in complex 17. All mass spectra are provided in Figures 4.2–4.5.

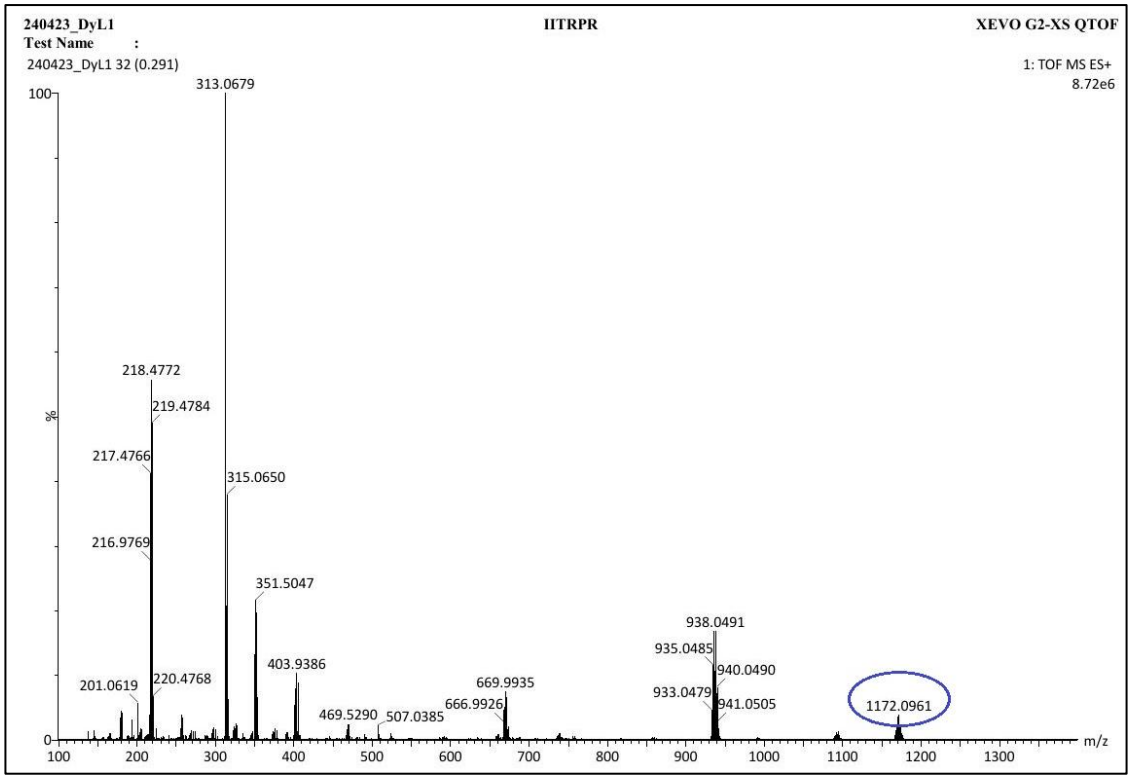

Figure 4.2 Mass spectrum of complex 12.

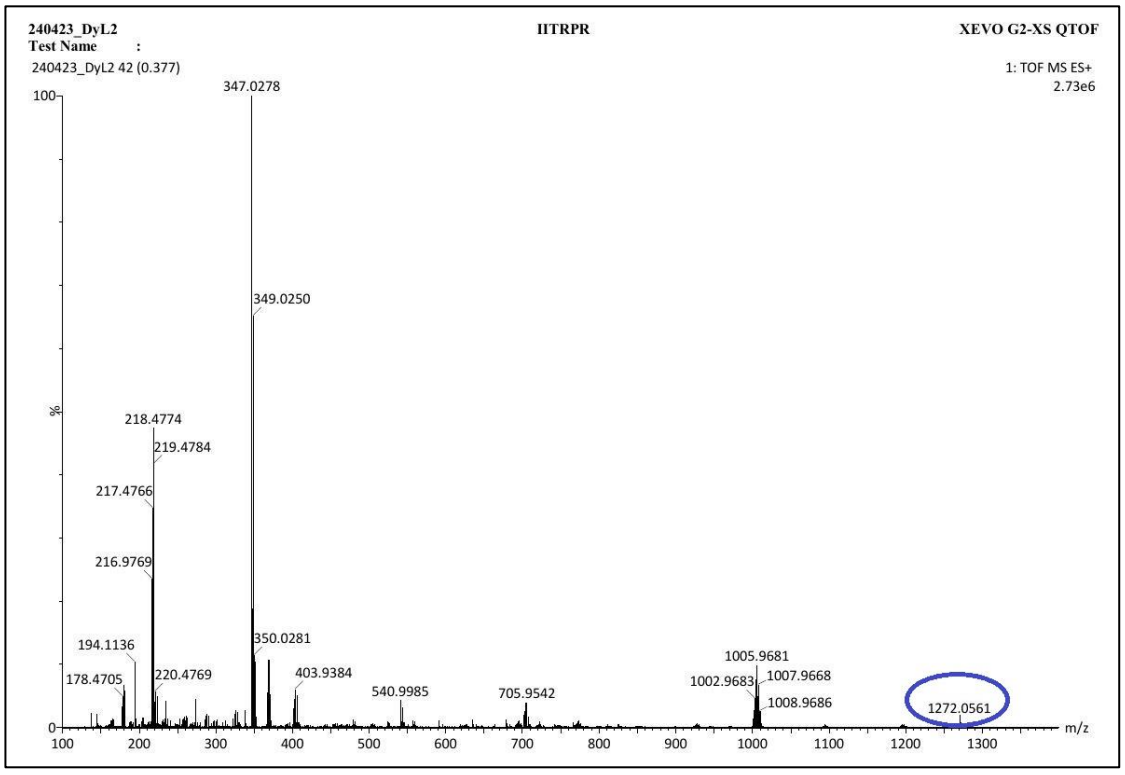

Figure 4.3 Mass spectrum of complex 13.

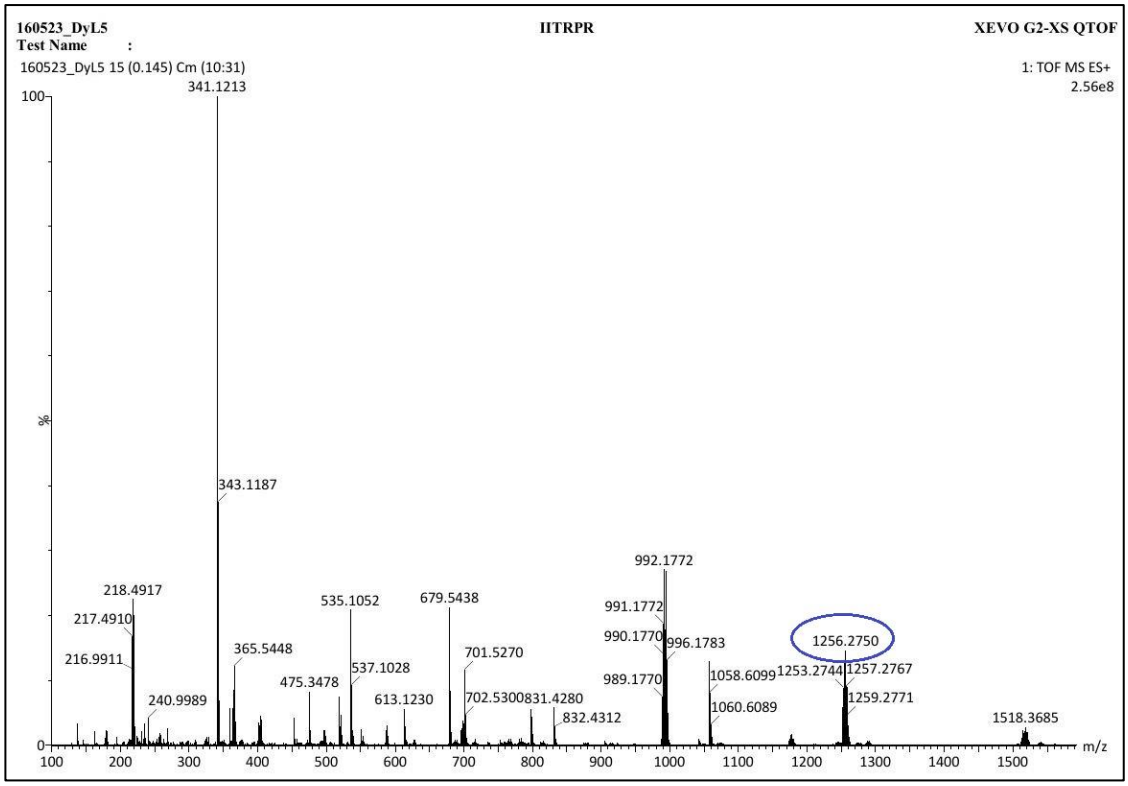

Figure 4.4 Mass spectrum of complex 16.

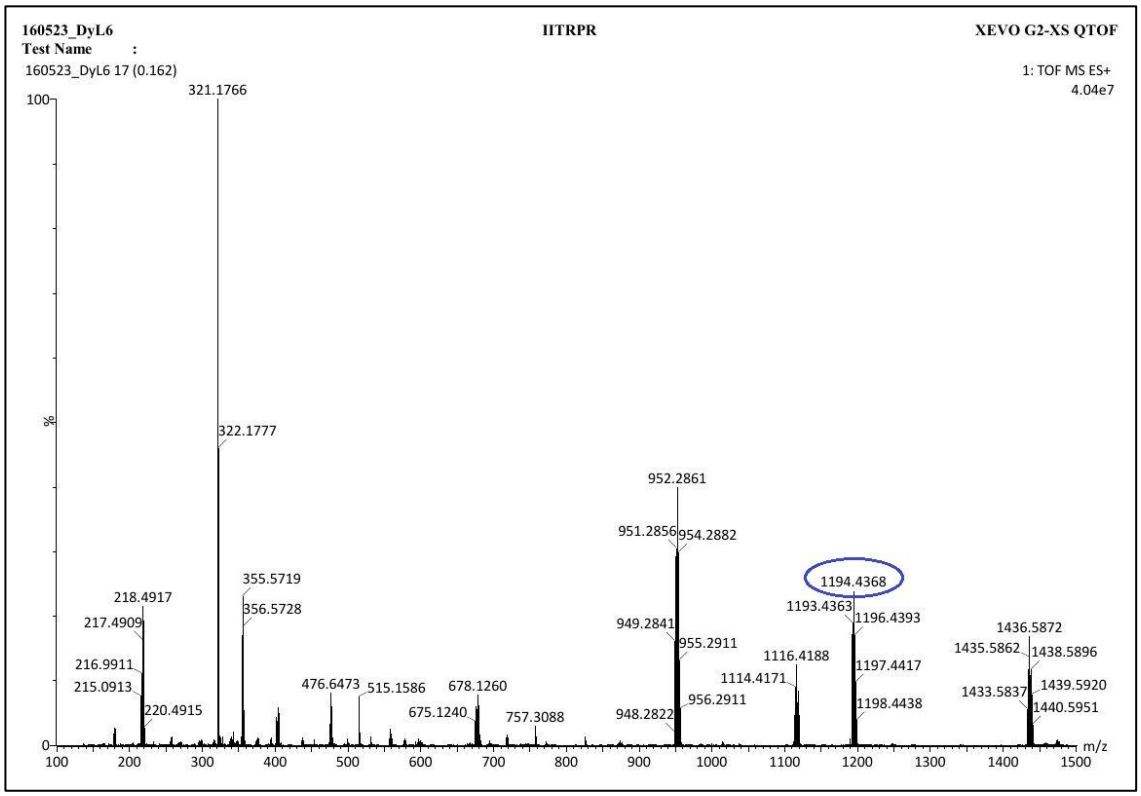

Figure 4.5 Mass spectrum of complex 17.

4.3.2 FTIR spectral analysis

All the Dysprosium complexes listed in Table 4.1 have one CH_3CH_2OH and one H_2O bound as monodentate ligands, as shown by the FTIR bands of the $\upsilon_{O\text{-}H(ethanol)}$ and $\upsilon_{O\text{-}H(water)}$ ligands, respectively. This is because all six complexes were synthesized using aqueous NaOH and hydrated Dysprosium nitrate salt as the starting material, and 100% ethanol was employed as the solvent throughout the process. The notable finding is a decrease in $\upsilon_{C=O(Benzoyl)}$ and $\upsilon_{C=O(acyl\text{-}pyz)}$ stretching of ligands during complexation due to charge donation to Dy-ion by O-atoms of acylpyrazolone. $\upsilon_{C=O(Benzoyl)}$ is falling from 1620 cm^{-1} of HL^1 to 1612 cm^{-1} of complex 12, 1624 cm^{-1} of HL^2 to 1613 cm^{-1} of complex 13, 1694 cm^{-1} of HL^3 to 1601 cm^{-1} of complex 14, 1621 cm^{-1} of HL^4 to 1613 cm^{-1} of complex 15, 1624 cm^{-1} of HL^5 to 1615 cm^{-1} of complex 16, and 1622 cm^{-1} of HL^6 to 1619 cm^{-1} of complex 17, Similar to this, $\upsilon_{C=O(acyl\text{-}pyz)}$ stretching becomes less when a complex is formed. Using the FTIR spectra of the complexes, which are shown in Figures 4.6–4.11, additional bands such as cyclic $\upsilon_{C=N}$, $\upsilon_{C=C}$, $\upsilon_{N–N}$, and $\upsilon_{C–H\ in\ plane\ deformations}$ were also assigned to all complexes.

Table 4.1 The FTIR values for Dysprosium complexes (in cm^{-1}).

Vibrations (in cm^{-1})	HL^1	Complex 12	HL^2	Complex 13	HL^3	Complex 14	HL^4	Complex 15	HL^5	Complex 16	HL^6	Complex 17
$\nu_{(O\text{-}H)}$ water	-	3063	-	3105	-	3034	-	3408	-	3109	-	3034
$\nu_{(O\text{-}H)}$ ethanol	-	2926	-	2972	-	2926	-	2923	-	2921	-	2921
$\nu_{(C=O)}{}^{A}$	1620	1612	1624	1613	1694	1601	1621	1613	1624	1615	1622	1619
$\nu_{(C=O)}{}^{B}$	1590	1592	1590	1589	1601	1504	1605	1581	1589	1588	1607	1597
cyclic $\nu_{(C=N)}$	1484	1498	1484	1479	1446	1480	1511	1488	1554	1480	1511	1489
$\nu_{aromatic(C\text{-}C)}$	1357	1371	1348	1366	1381	1378	1307	1370	1344	1365	1356	1372
$\nu_{(N\text{-}N)}$	1213	1155	1210	1158	1178	1159	1175	1134	1176	1135	1175	1147
C-H in plane deformation	1085	1072	1080	957	1071	1016	1067	1065	1080	1070	1066	1065

[A]Benzoyl group, [B]acyl-pyz

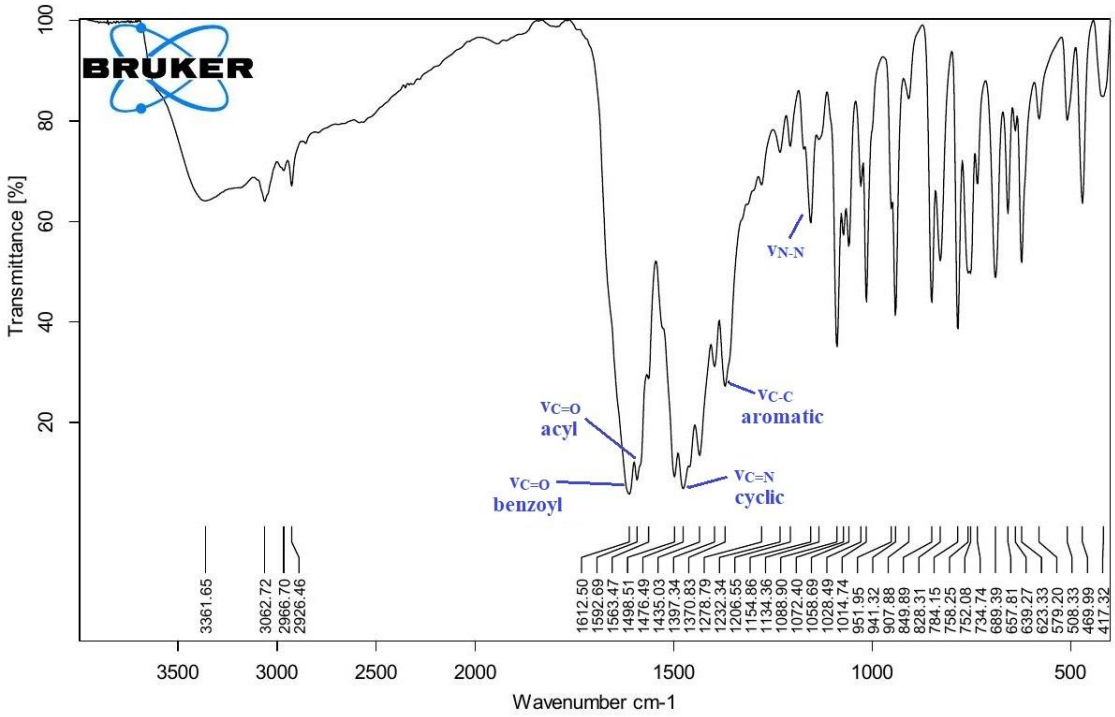

Figure 4.6 FTIR spectrum of complex 12.

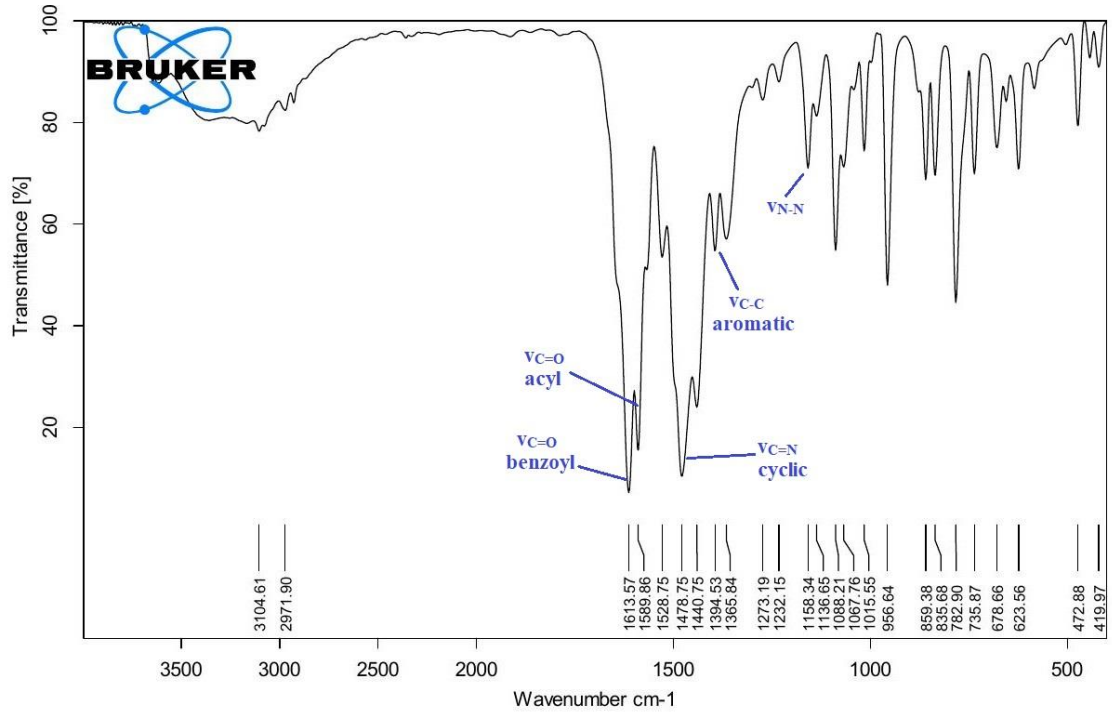

Figure 4.7 FTIR spectrum of complex 13.

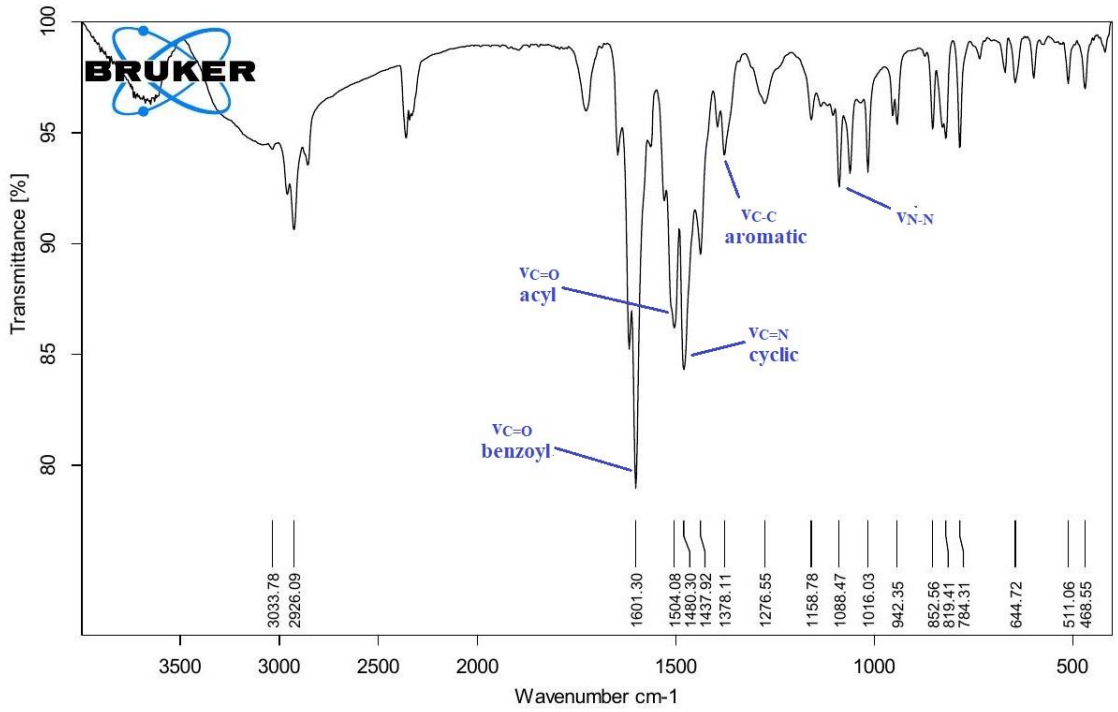

Figure 4.8 FTIR spectrum of complex 14.

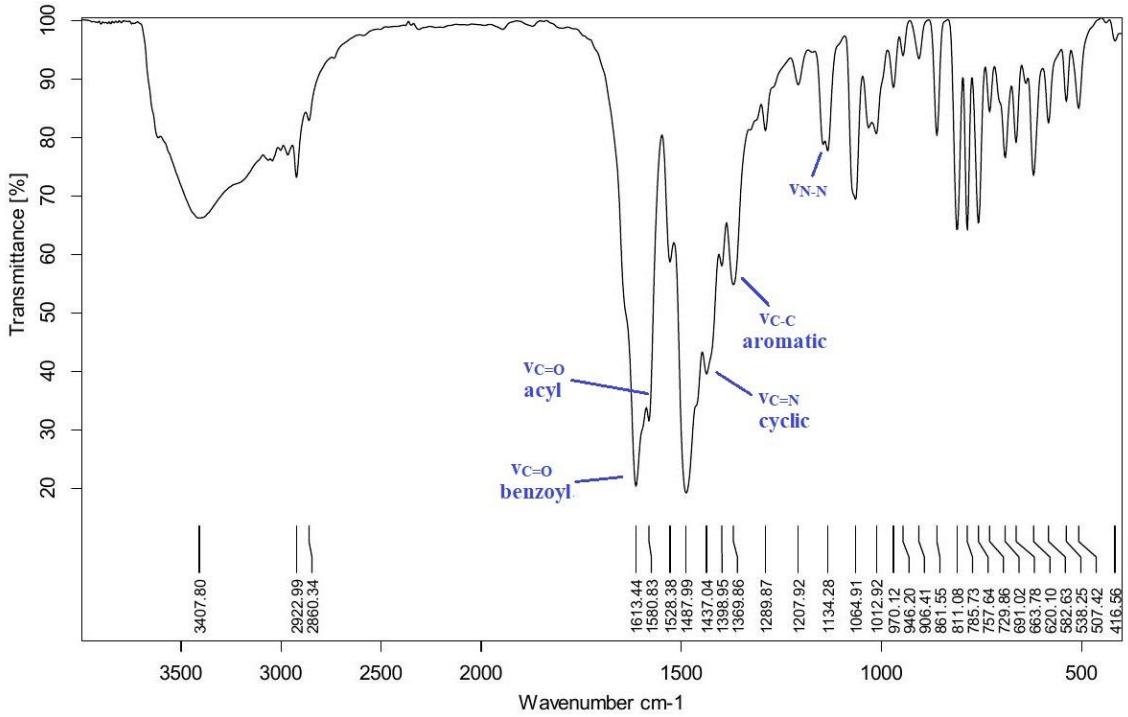

Figure 4.9 FTIR spectrum of complex 15.

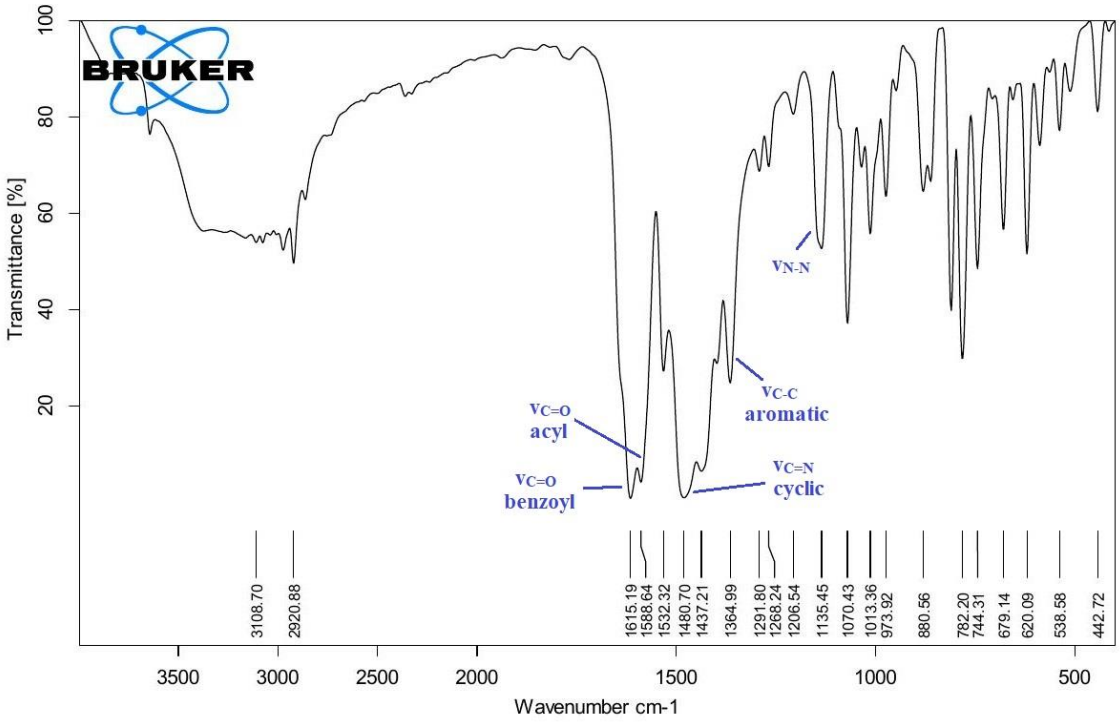

Figure 4.10 FTIR spectrum of complex 16.

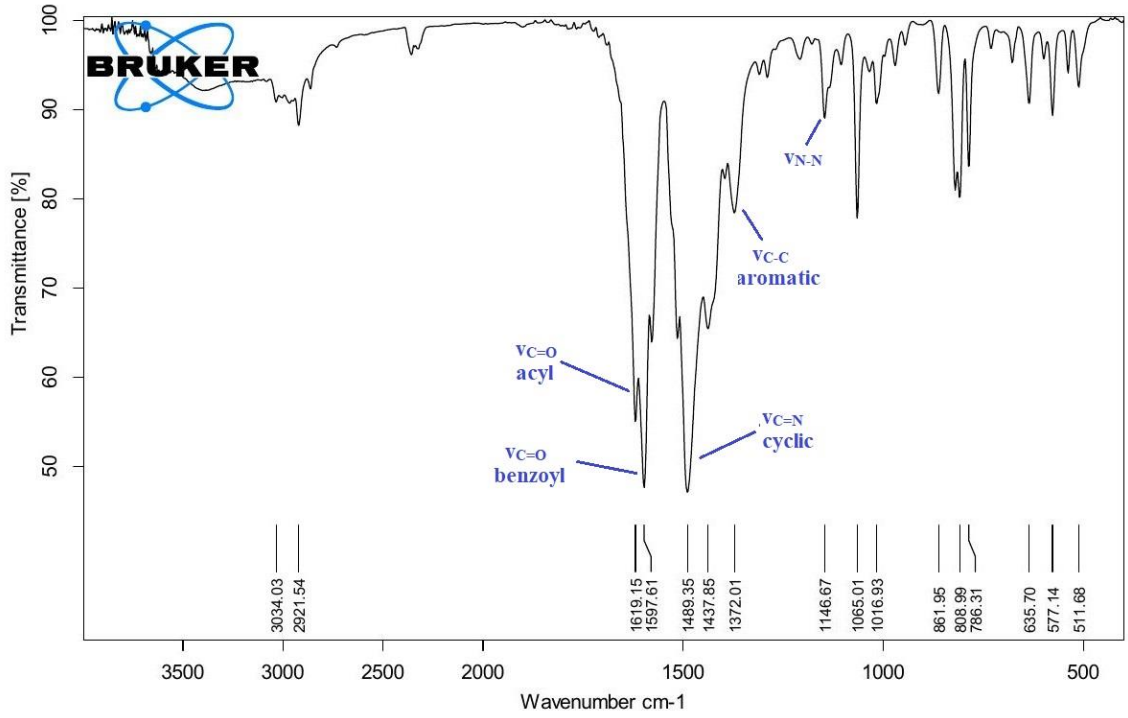

Figure 4.11 FTIR spectrum of complex 17.

4.3.3 Thermogravimetric analysis

Complexes were submitted to a thermal examination since thermal stability plays a significant role in determining their volatility. For the complexes 12, 13, 14, 15, 16, and 17, respectively, the TGA shows two degradation steps with overall mass losses of 41.7%, 45.1%, 44%, 44.1%, 48.1%, and 46.4%. The final substance, Dy_2O_3, is left behind. The first stage of degradation with mass loss of 5.6% for complex 12 (65.00 g), 5% for complex 13 (63.10 g), 5.2% for complex 14 (62.51 g), 5.6% for complex 15 (63.93 g), 5.1% for complex 16 (63.46 g), and 5.6% for complex 17 (66.28 g) complexes involves the loss of one H_2O (18 g) and one EtOH (46 g) molecules as coordinated solvents, however actual complex degradation happens above their melting points. The second stage of degradation with mass loss of 36.1% for complex 12, 40.1% for complex 13, 38.8% for complex 14, 38.5% for complex 15, 43% for complex 16, and 40.8% for complex 17 is due to the removal of three acylpyrazolone units. DTG curves show the maximum loss of 747.5, 743.2, 337.8, 750.7, 678.6, and 480.7 μg min^{-1} for complexes 12, 13, 14, 15, 16, and 17 at 426.9, 431.1, 428.9, 433.8, 439.2, and 431.6 °C, respectively. Figures 4.12–4.17 contain all thermogravimetric curves.

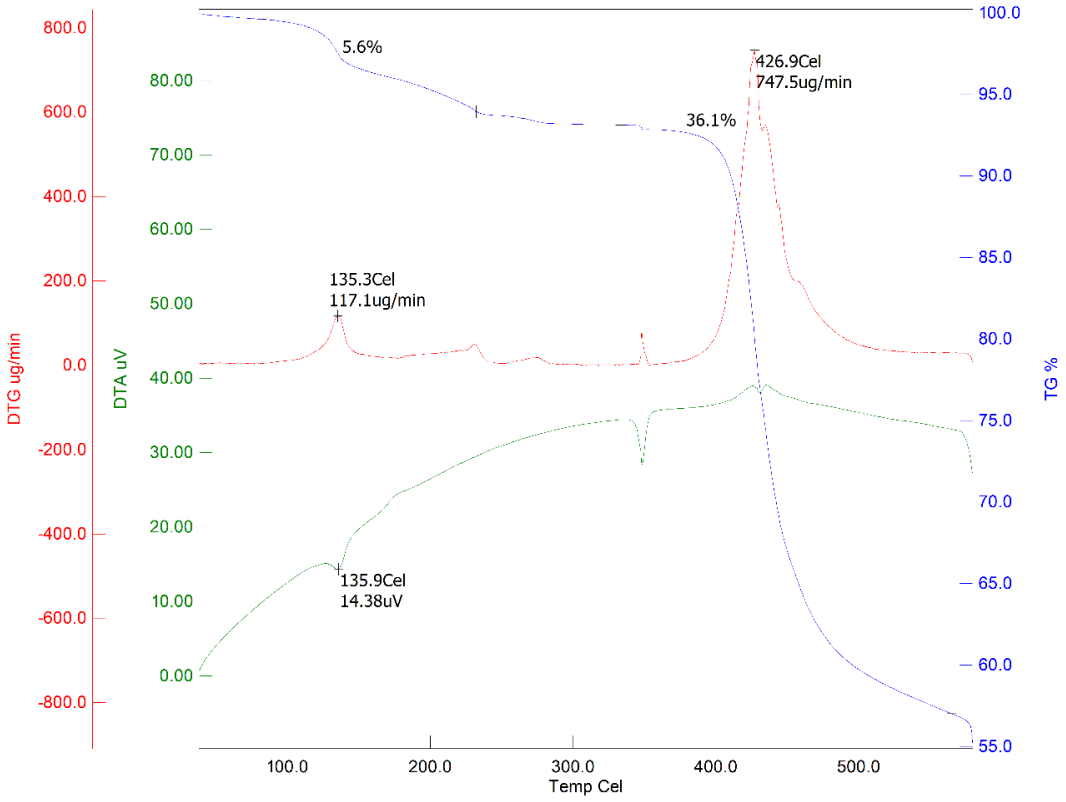

Figure 4.12 Thermogravimetric curve for complex 12.

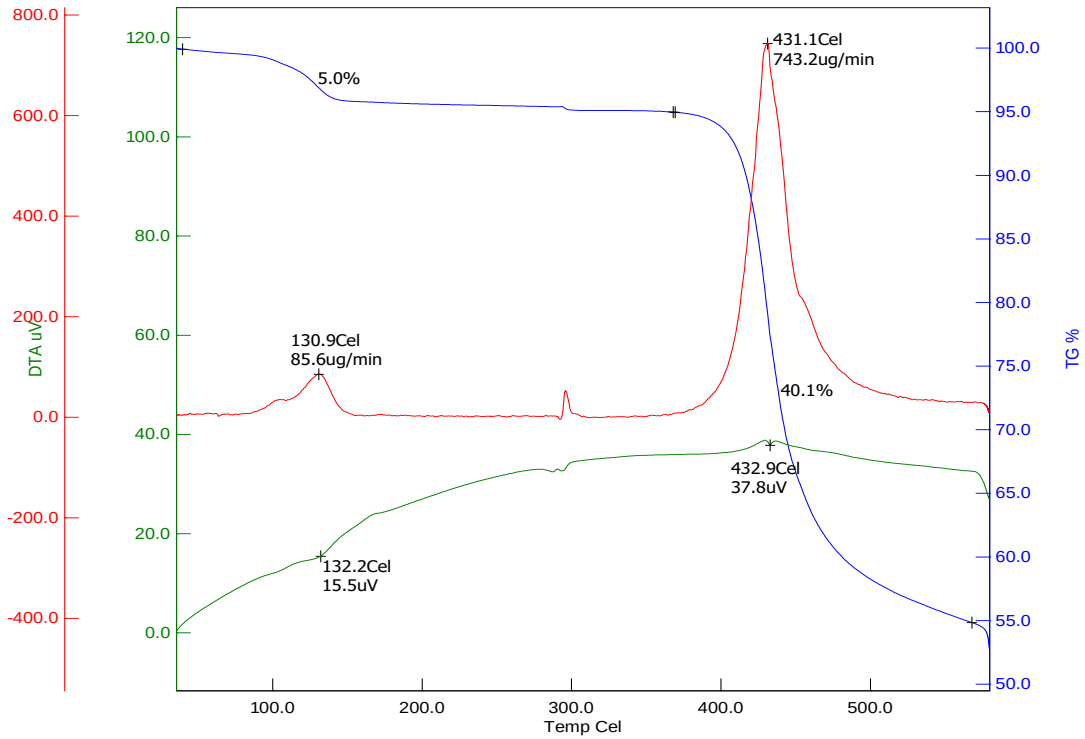

Figure 4.13 Thermogravimetric curve for complex 13.

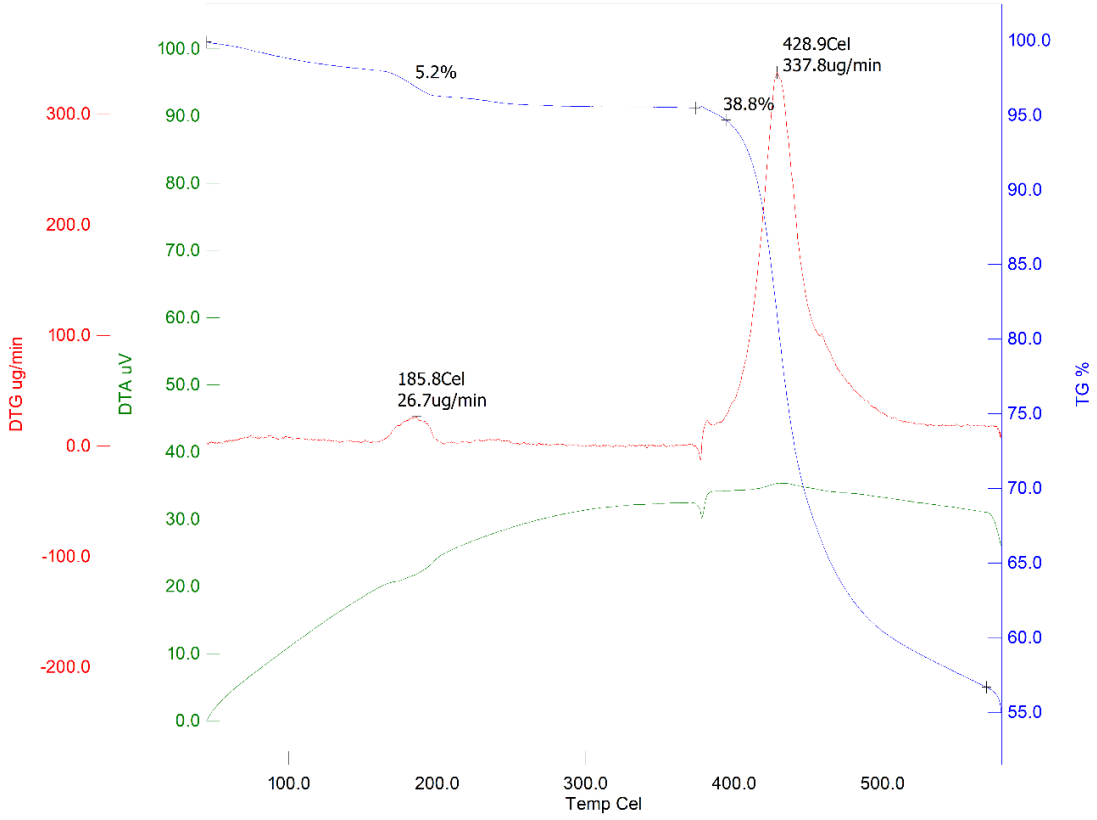

Figure 4.14 Thermogravimetric curve for complex 14.

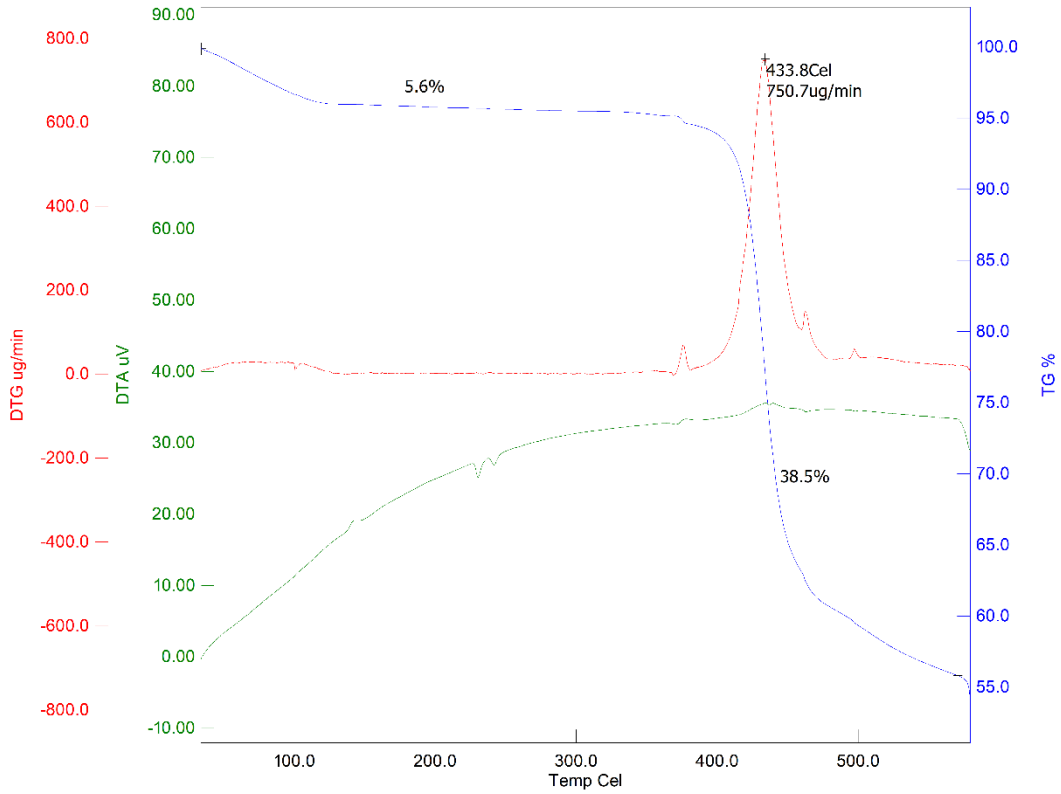

Figure 4.15 Thermogravimetric curve for complex 15.

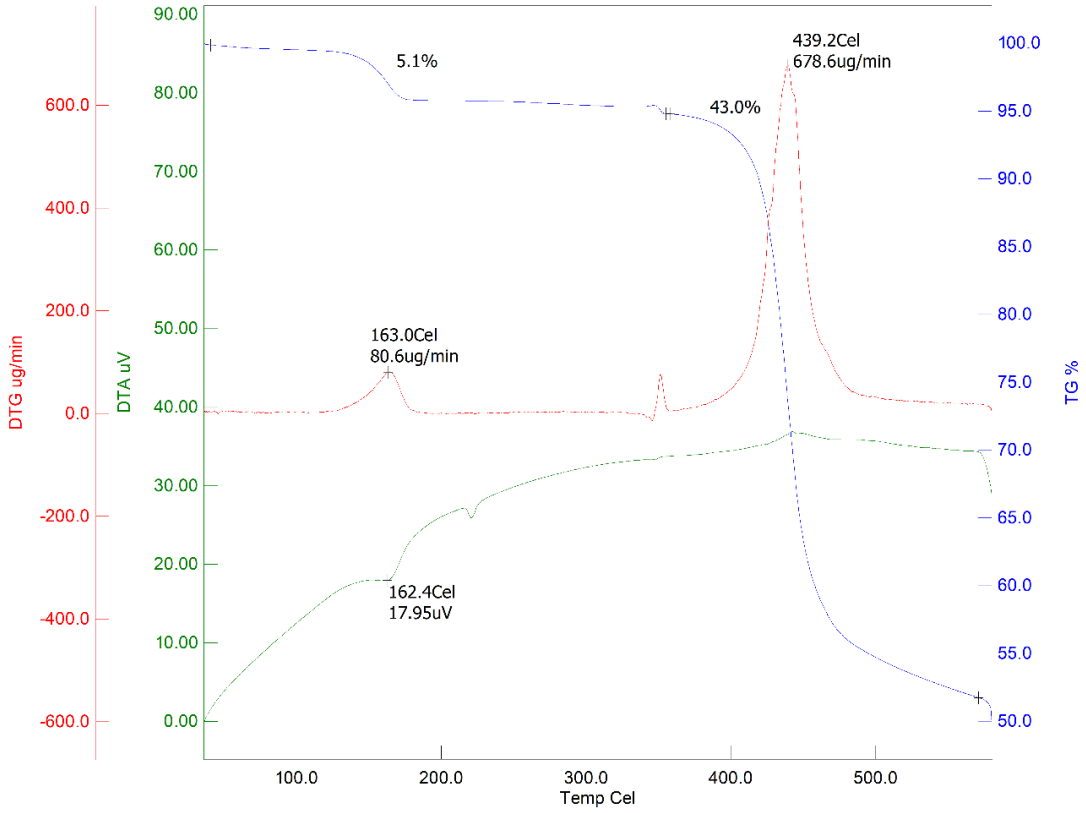

Figure 4.16 Thermogravimetric curve for complex 16.

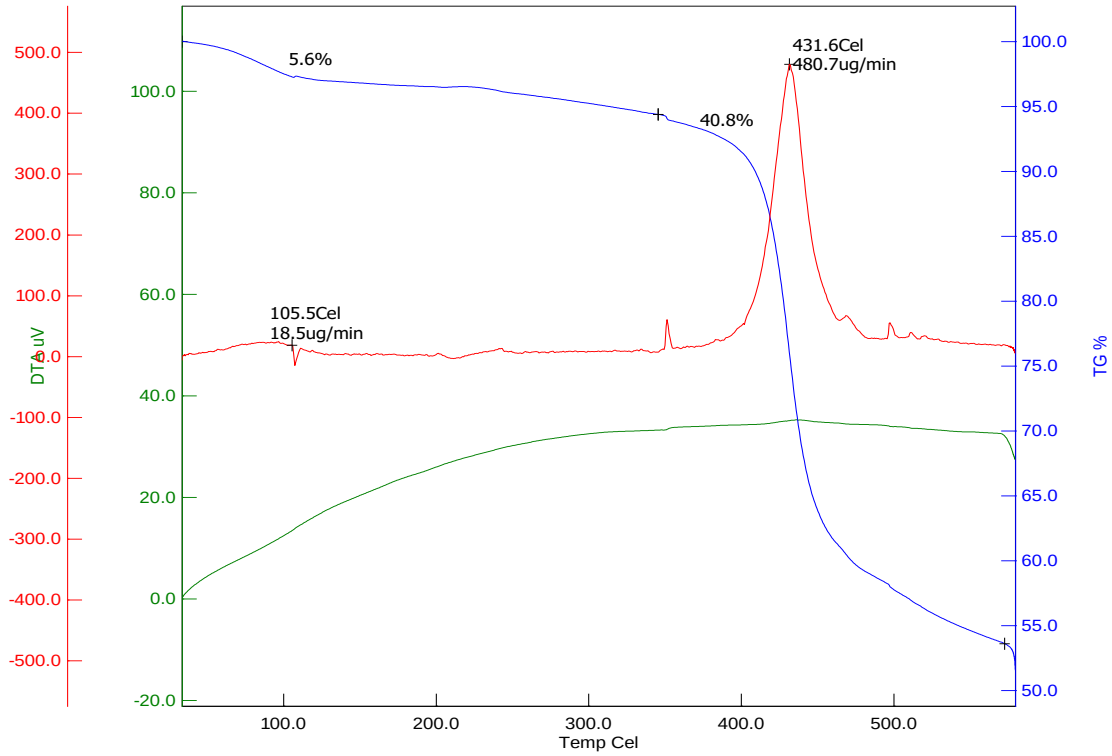

Figure 4.17 Thermogravimetric curve for complex 17.

4.3.4 Single crystal X-ray diffraction analysis

The bright pale-yellow plate-type crystals of complex 15 were obtained through recrystallization in DMF and slow evaporation technique. After obtaining the pale-yellow plate-type single crystals necessary for X-ray measurement, solid-state X-ray diffraction was used to determine the structure of the complex 15. The quality of crystals was poor, and a face-indexed absorption correction was not possible as the crystal was transparent and emersed in oil; thus, a multi-scan type absorption correction was applied. However, there were still significant peaks near the heaviest atoms. Generally, structurally characterized complexes of L^1–L^6 with Uranium and Neodymium show pentagonal bipyramidal and distorted square-antiprism geometry, as we discussed in the earlier Chapters. But like the reports of the Dysprosium acylpyrazolone complexes [21–24], the mononuclear complex 15 features an eight-coordinated core Dy(III) ion, which is surrounded by six L^4 ligand O-atoms (O1A, O2A, O3A, O4A, O5A, and O6A), and two DMF O-atoms (O7A and O8A). Around the centre Dy(III) ion, the eight O-atoms organize into a warped square-antiprism coordination polyhedron and complex crystallized in the *P c a 21* space group of the orthorhombic system (See Figure 4.18(a) and 4.18(b)). One potential ligand configuration, centred on the central atom, is shown in Fig. 4.18(c) [25].

The crystal packing of the complex satisfies the criteria of low energy movement between metal ions because the Dy-Dy distance is 14.414 Å [26]. Three L^4 ligands encounter the central Dysprosium ion as bidentate ligands, forming three chelating rings [27,28]. The top plane can be formed by joining O4A, O6A, and O1A atoms of the three different acylpyrazolone ligands and O8A of DMF. Similarly, the bottom plane can be formed by joining O2A, O3A, and O5A atoms of the three different acylpyrazolone ligands and O7A of DMF.

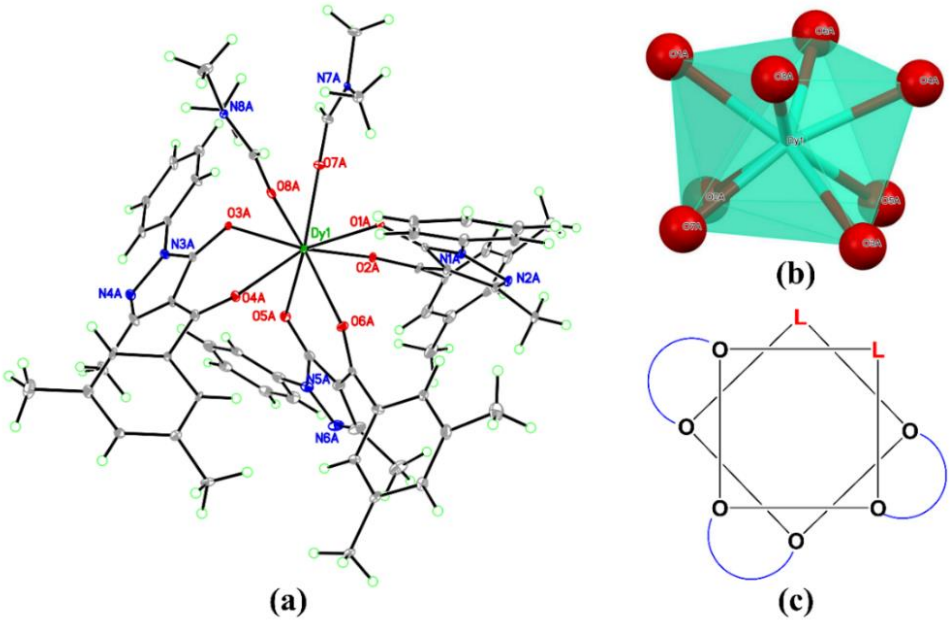

Figure 4.18 (a) ORTEP illustration with atoms labelling and 50% ellipsoid probability, **(b)** Polyhedral style presentation, and **(c)** Arrangement of square antiprism for complex 15.

Table 4.2 contains an overview of the crystallographic information and refinement information, while Table 4.3 lists the selected bond lengths and angles. Slight distortion in square antiprism is observed as O6A and O8A atoms are slightly above the upper plane, while O1A and O4A atoms are slightly below and on the opposite side, O2A, O3A atoms are slightly below the bottom plane, while O5A, O7A atoms are slightly above. The lengths of the C(11A)–O(2A), C(30A)–O(4A), and C(49A)–O(6A) bonds in the acyl group are 1.27(3) Å, 1.21(3) Å, and 1.26(3) Å, respectively, that is slightly higher than typical for C–O distance in ketones [29] (1.23 Å) due to O→Dy bonding. In comparison to Dy-O(acyl) bond lengths (2.381-2.421), Dy-O(pyrazolone) bond lengths (2.344-2.383) are slightly higher, indicating stronger covalency caused by the acyl group O-atoms. The bond lengths for the Dy-O7A and

Dy-O8A bonds are 2.403(14) Å and 2.378(15) Å, respectively, which demonstrate covalent binding and the influence of DMF solvent on the covalent character in the complex. The L^4 ligands form stable six-membered rings when they coordinate to the Dysprosium ion in its enol state; the sum of the internal angles for the three ligands is, respectively, 714.36, 705.65, and 706.76°. These angles are very near 720°, indicating that the six-membered rings are almost planar. Indicating some electron delocalization during complexation, the average $C{=}C_{pyz\text{-}ring}$ distance is 1.421 Å, which is in the middle of the usual C=C and C-C bond distances of 1.33 Å and 1.54 Å, respectively.

Table 4.2 Crystallographic structural refinement for complex 15.

Code	Complex 15
CCDC number	2271257
Empirical formula	$C_{63}H_{65}DyN_8O_8$
Formula weight	1224.73
Temperature	100(2) K
Wavelength	0.71073 Å
Crystal system	Orthorhombic
Space group	P c a 21
Unit cell dimensions	a = 13.3515(11) Å α= 90°, b = 30.082(2) Å β= 90°, c = 28.596(2) Å γ = 90°.
Volume	11485.2(15) $Å^3$
Z	8
Density (calculated)	1.417 Mg/m^3
Absorption coefficient	1.364 mm^{-1}
F(000)	5032
Final R indices [I>2sigma(I)]	R_1 = 0.1106, wR_2 = 0.2659
R indices (all data)	R_1 = 0.1272, wR_2 = 0.2788
Theta range for data collection	1.965 to 26.439°.
Index ranges	0<=h<=16, 0<=k<=17, 0<=l<=35
Reflection collected	23206
Independent reflections	23206
Completeness to theta = 25.242°	99.8 %
Absorption correction	None
Refinement method	Full-matrix least-squares on F^2
Goodness-of-fit on F^2	1.072
Data / restraints / parameters	23206 / 1637 / 1312

Table 4.3 Selected bond lengths(Å) and bond angles(°) for complex 15.

Atoms	Bond lengths	Atoms	Bond lengths	Atoms	Bond angles	Atoms	Bond angles
Dy(1)-O(1A)	2.344(14)	N(1A)-C(1A)	1.35(3)	O(1A)-Dy(1)-O(3A)	149.9(5)	O(5A)-Dy(1)-O(7A)	119.9(5)
Dy(1)-O(3A)	2.354(14)	N(1A)-C(5A)	1.44(2)	O(1A)-Dy(1)-O(8A)	75.9(5)	O(2A)-Dy(1)-O(7A)	74.3(5)
Dy(1)-O(8A)	2.378(15)	N(1A)-N(2A)	1.44(2)	O(3A)-Dy(1)-O(8A)	83.8(5)	O(1A)-Dy(1)-O(6A)	70.5(5)
Dy(1)-O(4A)	2.381(16)	N(2A)-C(3A)	1.31(3)	O(1A)-Dy(1)-O(4A)	119.8(5)	O(3A)-Dy(1)-O(6A)	138.0(5)
Dy(1)-O(5A)	2.383(15)	N(3A)-C(20A)	1.33(3)	O(3A)-Dy(1)-O(4A)	73.4(5)	O(8A)-Dy(1)-O(6A)	107.8(6)
Dy(1)-O(2A)	2.385(16)	N(3A)-C(24A)	1.43(2)	O(8A)-Dy(1)-O(4A)	72.8(5)	O(4A)-Dy(1)-O(6A)	72.2(6)
Dy(1)-O(7A)	2.403(14)	N(3A)-N(4A)	1.45(3)	O(1A)-Dy(1)-O(5A)	133.2(5)	O(5A)-Dy(1)-O(6A)	74.3(6)
Dy(1)-O(6A)	2.421(16)	N(4A)-C(22A)	1.32(3)	O(3A)-Dy(1)-O(5A)	74.4(5)	O(2A)-Dy(1)-O(6A)	83.0(6)
O(1A)-C(1A)	1.29(3)	N(5A)-N(6A)	1.32(3)	O(8A)-Dy(1)-O(5A)	145.6(5)	O(7A)-Dy(1)-O(6A)	146.3(6)
O(2A)-C(11A)	1.27(3)	N(5A)-C(43A)	1.41(3)	O(4A)-Dy(1)-O(5A)	75.6(6)	C(1A)-O(1A)-Dy(1)	122.8(13)
O(3A)-C(20A)	1.28(3)	N(5A)-C(39A)	1.45(3)	O(1A)-Dy(1)-O(2A)	73.7(5)	C(11A)-O(2A)-Dy(1)	133.0(14)
O(4A)-C(30A)	1.21(3)	N(6A)-C(41A)	1.32(4)	O(3A)-Dy(1)-O(2A)	112.9(5)	C(20A)-O(3A)-Dy(1)	123.3(13)
O(5A)-C(39A)	1.24(3)	N(7A)-C(58A)	1.32(3)	O(8A)-Dy(1)-O(2A)	141.9(5)	C(30A)-O(4A)-Dy(1)	134.8(15)
O(6A)-C(49A)	1.26(3)	N(7A)-C(60A)	1.46(3)	O(4A)-Dy(1)-O(2A)	143.6(5)	C(39A)-O(5A)-Dy(1)	124.9(16)
O(7A)-C(58A)	1.26(3)	N(7A)-C(59A)	1.47(3)	O(5A)-Dy(1)-O(2A)	72.2(5)	C(49A)-O(6A)-Dy(1)	134.3(16)
O(8A)-C(61A)	1.24(3)	N(8A)-C(61A)	1.33(3)	O(1A)-Dy(1)-O(7A)	79.3(5)	C(58A)-O(7A)-Dy(1)	167.3(13)
C(1A)-C(2A)	1.39(3)	N(8A)-C(62A)	1.42(4)	O(3A)-Dy(1)-O(7A)	74.9(6)	C(61A)-O(8A)-Dy(1)	166.2(15)
C(21A)-C(22A)	1.41(3)	N(8A)-C(63A)	1.45(3)	O(8A)-Dy(1)-O(7A)	78.0(5)	C(1A)-N(1A)-C(5A)	134.1(17)
C(40A)-C(41A)	1.47(4)	C(2A)-C(3A)	1.39(3)	O(4A)-Dy(1)-O(7A)	138.6(6)	C(1A)-N(1A)-N(2A)	111.2(17)

A slow evaporation technique obtained bright pale-yellow plate-type crystals of complex 15. Attempts to get x-ray quality crystals of the other five complexes were proved futile. Therefore, a simulated pattern was obtained for complex 15 from the single crystal data, and the same was compared with the pattern obtained experimentally from the powder XRD experiment of complexes 12–17. The simulated pattern of complex 15 matches well with the experimental pattern for all six complexes, as shown in Figure 4.19. This confirms that all the complexes have similar geometry and structure. This also ensures the structure obtained from a single crystal represents the bulk of the complexes. In the XRD graph, a sharp band is observed with maxima in the range 2θ = 5 to 10°, indicating that the complexes are crystalline.

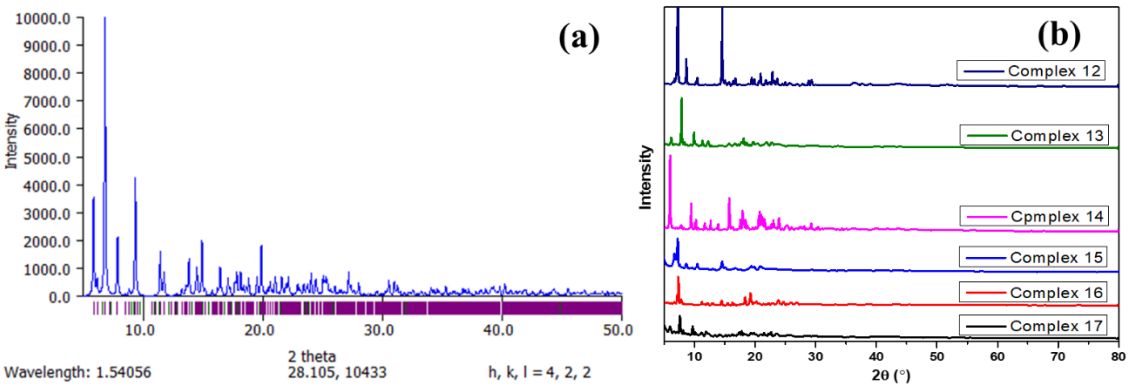

Figure 4.19 Comparison between (a) simulated powder XRD pattern for complex 15 crystal and (b) experimental powder XRD patterns for complexes 12–17.

4.3.5 Hirshfeld surface area analysis

Hirshfeld surface analysis was performed using the Crystal Explorer 17.5 program to demonstrate the numerous interactions present in a crystal structure. The HS is derived from the complex 15 crystal and displayed by the d_{norm}, accumulating exterior and interior distances (d_e and d_i). The surfaces of the 3D d_{norm}, d_i, d_e, curvedness, shape index, and fragment patch are explained in Figure 4.20, together with the 2D-FP plot. Red dots on d_{norm} HS represent closer short interactions. The total number of HS interactions with nearby complex 15 molecules (NBs) is presented in graphical form in Figure 4.21.

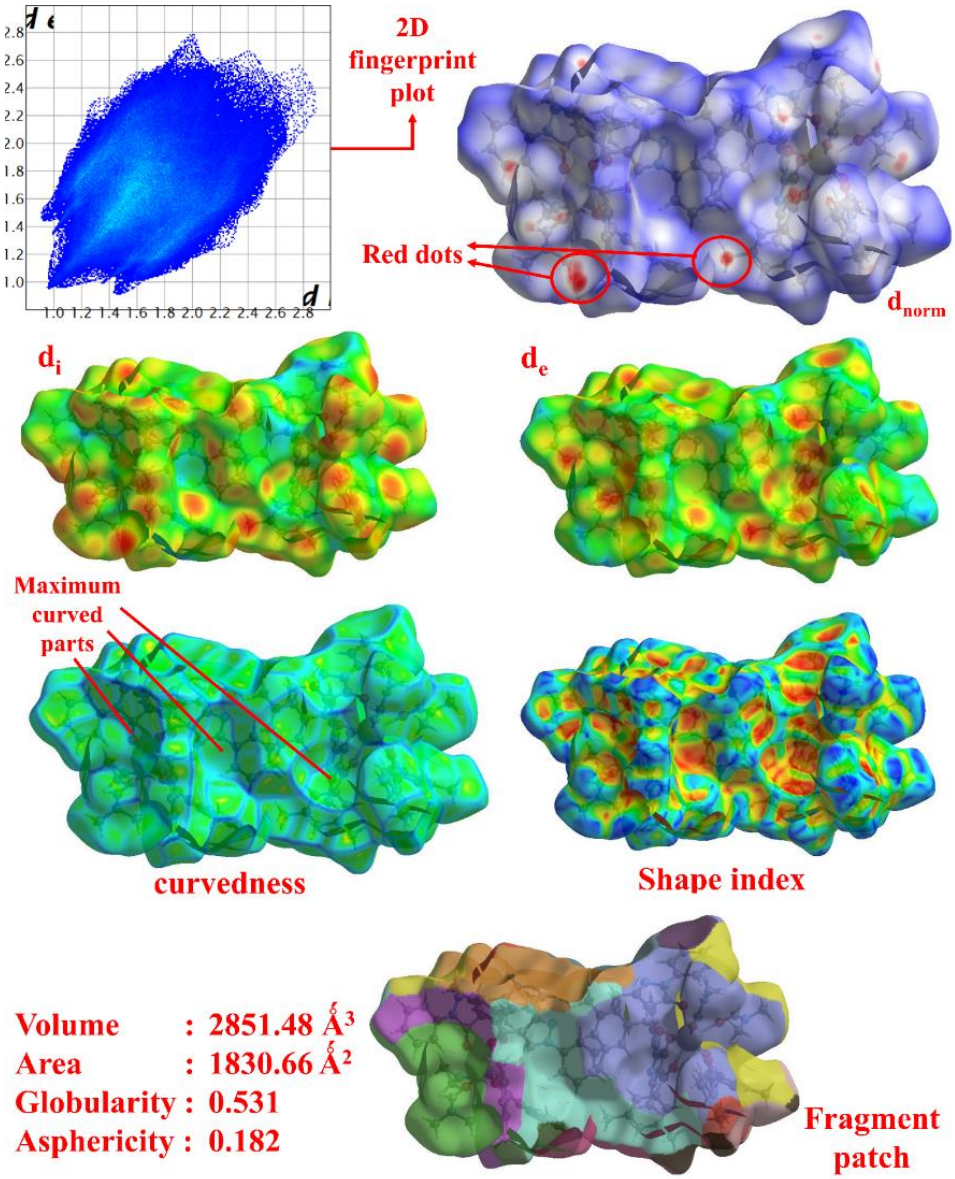

Figure 4.20 2D-FP plot and 3D d_{norm}, d_i, d_e, curvedness, shape index, and fragment patch surfaces for complex 15.

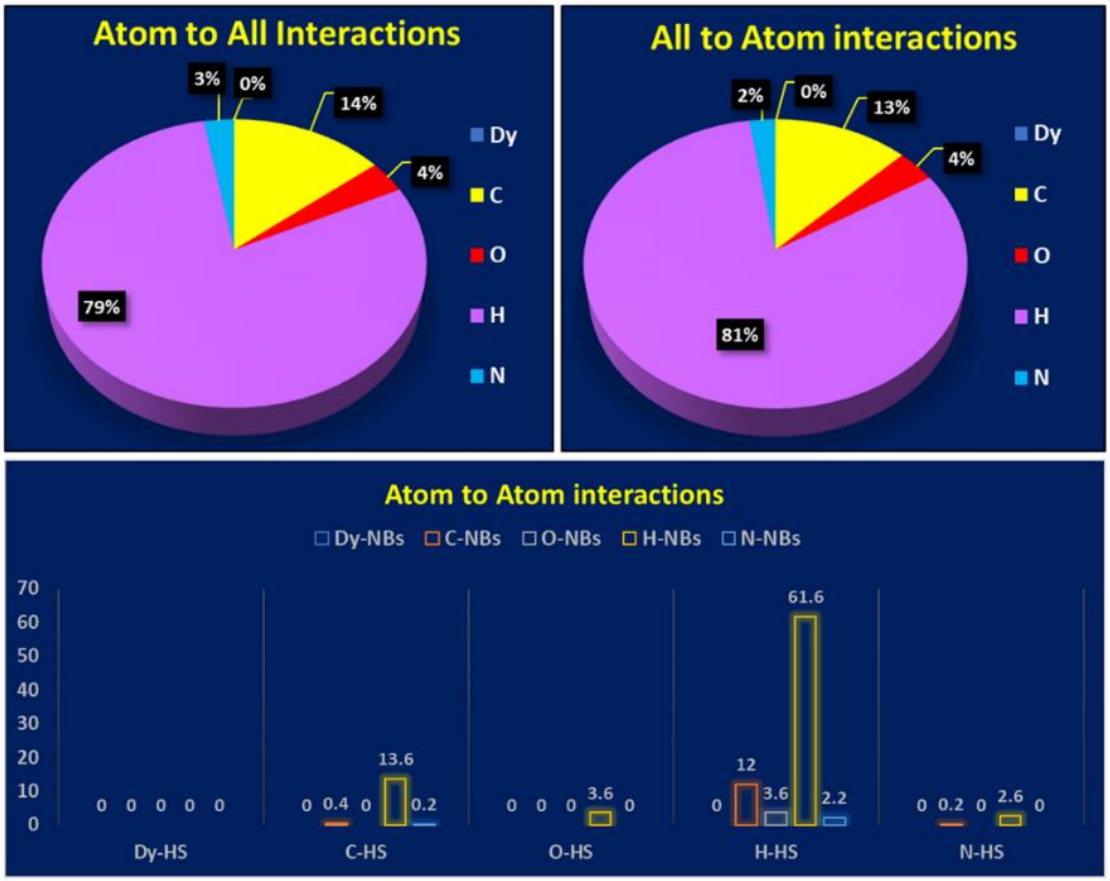

Figure 4.21 Graphical presentation of Hirshfeld Percentage interactions.

The interactions $H_{(HS)}\cdots H_{(NBs)}$, $H_{(HS)}\cdots All_{(NBs)}$, and $All_{(HS)}\cdots H_{(NBs)}$ showing the most frequent interactions, contributing respectively 61.6, 79.4, and 81.4%. Due to the large amounts of carbon and hydrogen in the HS, C···H interactions are the second most common interactions and account for 13.6% of the overall HS region. Figure 4.22 displays all required 2D-FP graphs. The curvy region on the curvedness map of 5-membered pyrazole rings denotes π-π stacking, strengthening the lattice along with the red dots in the d_{norm}. The non-existence of any Dy-all, all-Dy, or Dy-Dy interactions within the complex indicates that Dysprosium does not exhibit any additional interactions with the neighbouring molecules. According to shape-index maps, the concave appearance of O-atoms of ligands has manifested as an opaque orange tint having lower than zero shape-index value, providing proof of coordination interactions.

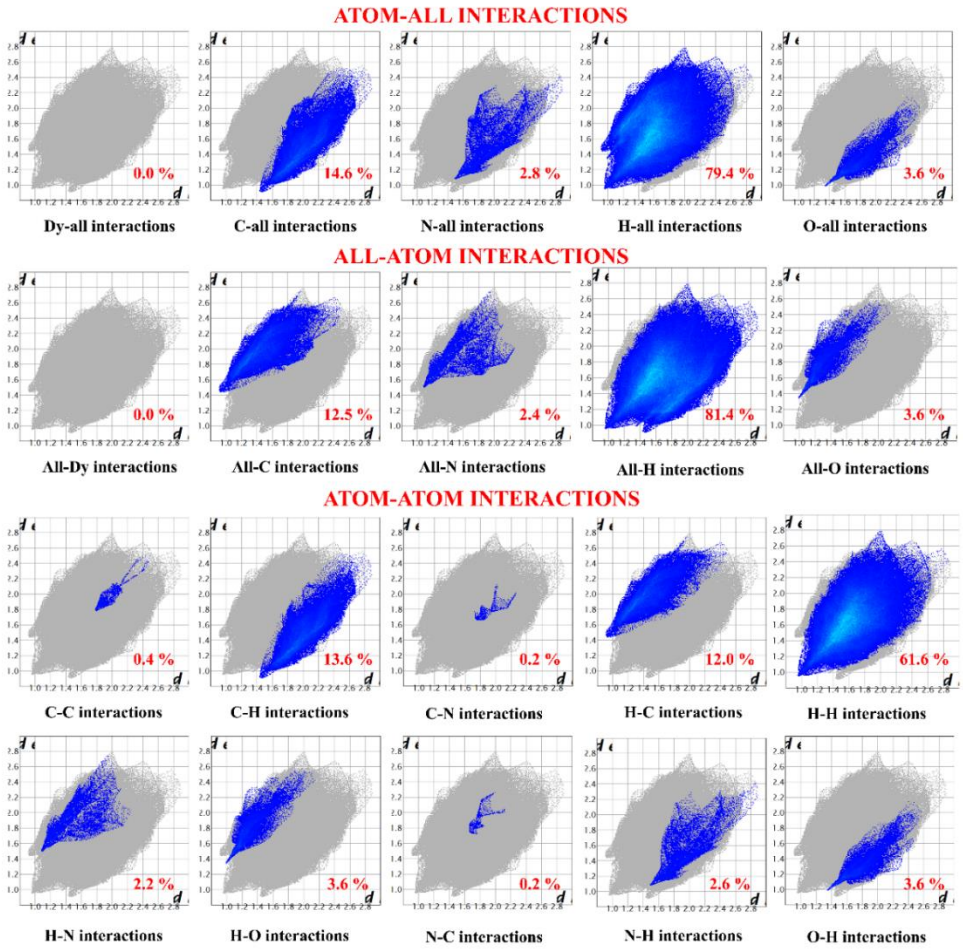

Figure 4.22 2D Fingerprint map for complex 15.

4.3.6 Electronic spectral analysis

All the synthesized complexes are soluble in various solvents, and the electronic or UV-Vis spectra of 10^{-6} M solution of these complexes were obtained in the chloroform, DMF and DMSO solvents. The outcomes of the spectra are shown in Figure 4.23. The spectra of ligands and complexes display a consistent pattern in both solvents. With their quick solvent transfer rate and remarkably low crystal field stabilization energy, these complexes can achieve more excellent coordination geometries [30,31]. The absorption bands corresponding to the n→π* and π→π* transitions are observed below 300 nm wavelength in both ligands and complexes. The additional broad and low intense peaks in the 350–400 nm range due to ligand to metal charge transfer is observed in DMF and DMSO solvents. This may be due to the replacement of DMF and DMSO solvents with coordinated solvents to promote charge transfer. The change in the band shape of absorption peaks is observed, as shown in Figure 4.23, and displays variation when exposed to various solvents [32,33].

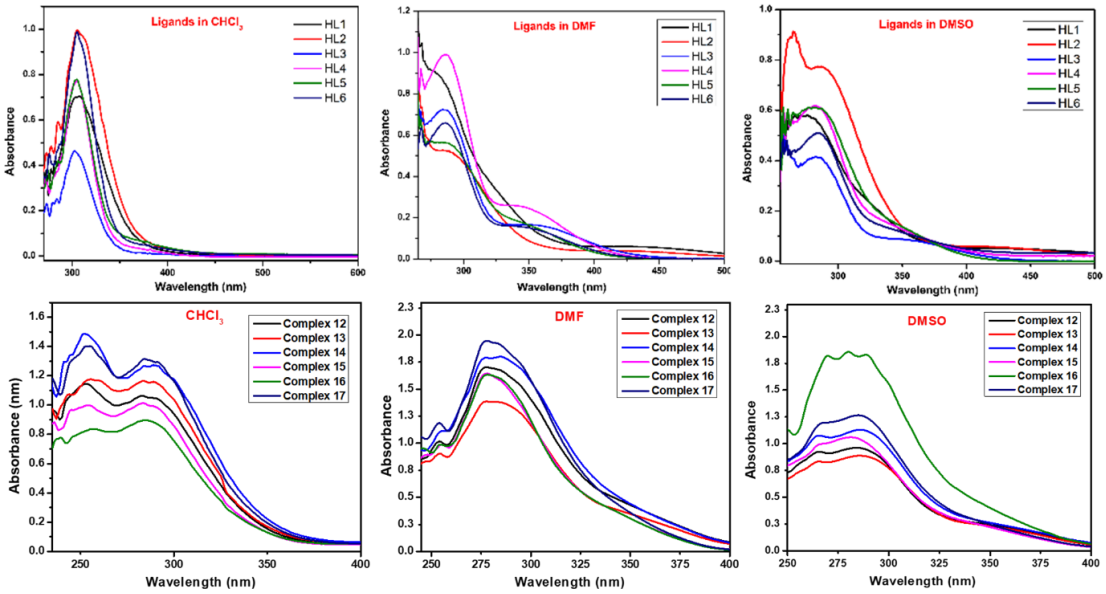

Figure 4.23 Electronic UV-Vis spectra of L^1–L^6 ligands and complexes 12–17 in $CHCl_3$, DMF, and DMSO solvents.

4.3.7 Fluorescence Emission Analysis

Using an excitation wavelength of 260 nm, the solid-state emission spectra of all six complexes depicted in Figure 4.24 were produced. $^4F_{9/2}\rightarrow{}^6H_{15/2}$ is a magnetic-dipole (MD) transition, and for that, the initial emission peak occupies the vicinity of blue and is observed around 470 and 490 nanometres. In this vicinity, the possibility of ion-ion cross-relaxation processes exists, and an integrated transfer from the $^4F_{9/2}\rightarrow{}^6H_{15/2}$ results in a polarised emission of a dual peak for a seemingly single transition [33,34]. The most significant peak, which indicates a transition from $^4F_{9/2}\rightarrow{}^6H_{13/2}$, occurs in the yellow zone between 510 and 530 nm. This transition is hyper-sensitive and is caused by a forced electric dipole (ED) highly reliant on the surroundings. The highest intensity of this transition is due to the low symmetric position of Dy^{3+} and is caused by the distorted square anti-prismatic geometry of complexes. The variance in intensity between ED and MD suggests a less asymmetric environment [35]. For the complexes 12, 13, 14, 15, 16, and 17, respectively, the Y/B (yellow to blue) ratio was found to be 1.58, 2.72, 1.35, 1.87, 4.11, and 3.22, and it is greater than unity (Y/B>1), indicating an increased level of Dy-O covalency. The $^4F_{9/2}\rightarrow{}^6H_{11/2}$ transition between 675-705 nm causes the weakest intensity peak to be in the red zone. Compared to published works [35–37], the $^4F_{9/2}\rightarrow{}^6H_{9/2}$,$^4F_{11/2}$ transition, which occurs in the near-infrared band between 750 and 800 nm, exhibits a considerable increase in intensity.

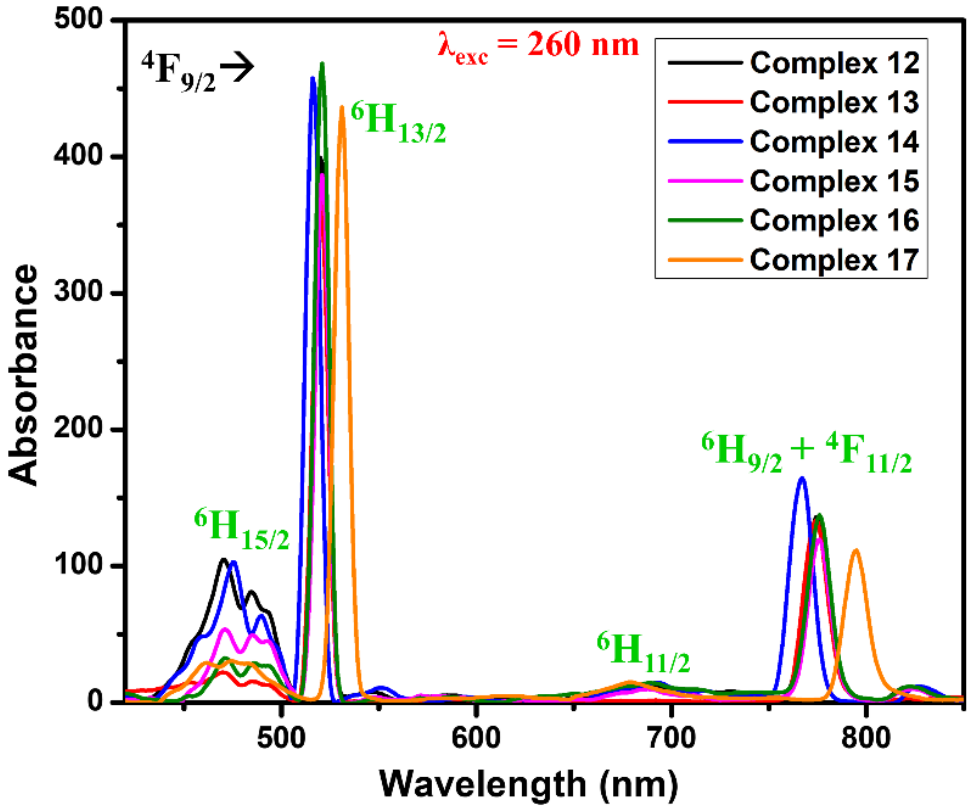

Figure 4.24 Fluorescence emission spectra of Dysprosium-acylpyrazolone complexes.

The widely recognized energy diagram is reported [38], shown in Figure 4.25, illustrates how energy is absorbed by the acylpyrazolone ligand, known as the "CL (central ligand)", transferred to the metal ion, and then returned to the ground state. The main ideas about the emission process of Dysprosium ions can be explained using this diagram. Energy travels through a path that begins with the central ligand absorbing energy into its excited singlet state, which is subsequently transferred to a triplet state by the ISC before arriving at the Dy(III) ion's energy levels. The functional group connected to the phenyl rings of acylpyrazolone, a NL (neutral ligand) that provides stability, fluorescence efficacy, absorption efficacy, and LMCT efficacy, is seen to have an impact on this light energy conversion diagram, which is also referred to as the "antenna effect".

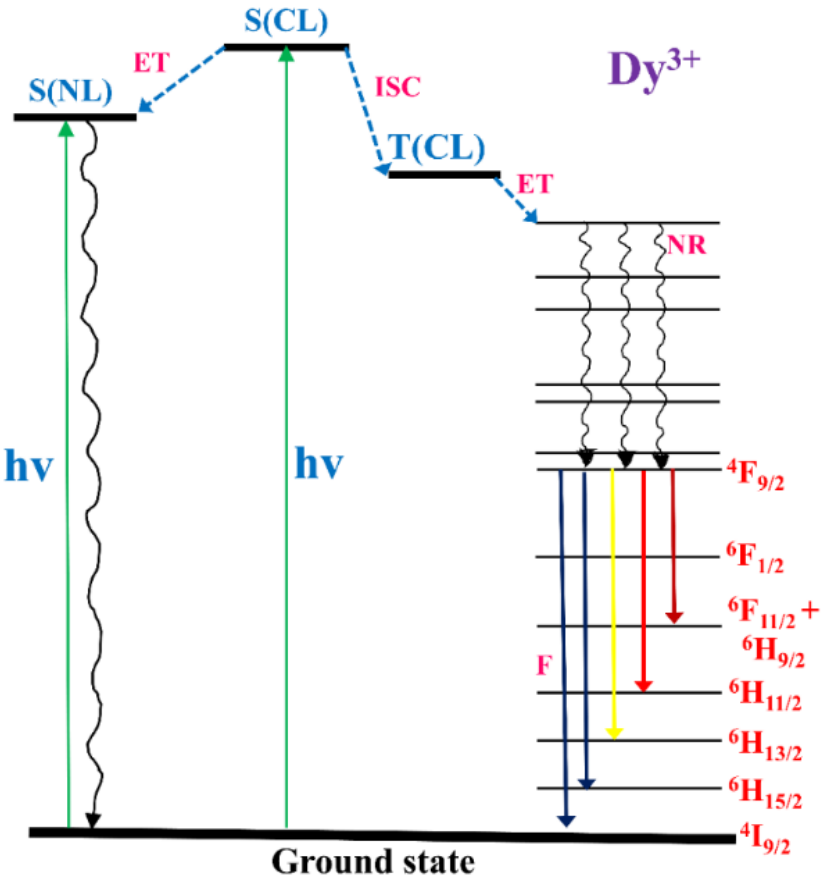

Figure 4.25 "Antenna effect" diagram showing the mechanism of the emission process in Dysprosium-acylpyrazolone complexes.

4.4 Conclusions

The main goals of the present research aimed to (i) synthesize six distorted square antiprismatic Dy(III)-acylpyrazolone complexes with structural characterization, (ii) study their emission transition peaks and show how the hypersensitive transitions and Y/B ratio responds to structural variations between the ligand in several complexes, and (iii) show the impact of various coordinating and non-coordinating solvents. Six Dysprosium-acylpyrazolone complexes 12–17 had eight-coordinated distorted square antiprism geometry held in space by three σ-donating acylpyrazolone ligands and two solvent molecules. The structure of all six complexes was also investigated using ESI-mass, FT-IR, thermogravimetric, powder XRD, UV-Vis and single-crystal X-ray diffraction methods. Initially, complex formation was

confirmed from FT-IR by observing a decrease in $\upsilon_{C=O(Benzoyl)}$ and $\upsilon_{C=O(acyl\text{-}pyz)}$ stretching of ligands during complexation. Compatibility with the $[Dy(L)_2(EtOH)(H_2O)]$ geometry was confirmed using ESI-mass, single crystal X-ray diffraction, and powder XRD patterns. Statistical and graphical analysis of secondary surface interactions were analyzed from Hirshfeld surface analysis. Four transitions, their type, and the Y/B ratio corresponding to different regions were examined using solid-state emission spectra. The transitions $^4F_{9/2} \rightarrow {}^6H_{15/2}$ and $^4F_{9/2} \rightarrow {}^6H_{13/2}$ are observed in the blue and yellow regions, respectively, and their Y/B ratio is greater than unity (Y/B>1), indicating an increased level of Dy-O covalency. The functional group attached to the phenyl rings of acylpyrazolone, an NL (neutral ligand) that provides stability, fluorescence efficacy, absorption efficacy, and LMCT efficacy, has a significant impact on the intensity of solid-state emission spectra as seen in antenna effect energy diagrams. The potential to modify the chemical and spectroscopic properties of acylpyrazolone to synthesize multi-dentate Dy(III) complexes, which have particular appeal in a wide range of potential applications in the disciplines of material sensing and scanning that could assist in the understanding of biological mechanisms or diagnosing of diseases.

References

[1] F. Marchetti, C. Pettinari, R. Pettinari, Acylpyrazolone ligands: Synthesis, structures, metal coordination chemistry and applications, Coord Chem Rev 249 (2005) 2909–2945. https://doi.org/10.1016/j.ccr.2005.03.013.

[2] L. Cisse, A. Djande, M. Capo-Chichi, F. Delattre, A. Saba, J.-C. Brochon, S. Sanouski, A. Tine, J.-J. Aaron, Fluorescence Quenching of Two Coumarin-3-carboxylic Acids by Trivalent Lanthanide Ions, J Fluoresc 27 (2017) 619–628. https://doi.org/10.1007/s10895-016-1990-1.

[3] I. Ameen, A.K. Tripathi, R.L. Mishra, A. Siddiqui, U.N. Tripathi, Aging effect on bonding properties of fluorescent neodymium materials, Karbala International Journal of Modern Science 4 (2018) 258–273. https://doi.org/10.1016/j.kijoms.2018.05.001.

[4] I. Ameen, A. Kumar Tripathi, R. Laxmi Mishra, A. Siddiqui, U. Nath Tripathi, Luminescent, optical, magnetic and metamaterial behavior of cerium complexes, J Saudi Chem Soc 23 (2019) 725–739. https://doi.org/10.1016/j.jscs.2018.12.003.

[5] U.P. Singh, N. Singh, R. Varshney, P. Roy, R.J. Butcher, Synthesis of Fluorescent Nanoscale Salts/Metal–Organic Frameworks for Live-Cell Imaging, Cryst Growth Des 18 (2018) 2804–2813. https://doi.org/10.1021/acs.cgd.7b01574.

[6] J. Yang, W. Ma, N. Jie, R. Han, Y. Han, A New Fluorimetric Reagent for Determining Trace Amounts of Aluminium(III), Microchemical Journal 54 (1996) 41–47. https://doi.org/10.1006/mchj.1996.0074.

[7] D.-J. Qian, W.-N. Leng, Y. Zhang, Z. Chen, J. Van Houten, A study of the fluorescence of some newly synthesized europium complexes with pyrazolone derivatives, Spectrochim Acta A Mol Biomol Spectrosc 56 (2000) 2645–2651. https://doi.org/10.1016/S1386-1425(00)00306-1.

[8] C. Pettinari, F. Marchetti, A. Cingolani, A. Drozdov, I. Timokhin, S.I. Troyanov, V. Tsaryuk, V. Zolin, Syntheses, structural and spectroscopic investigation (IR, NMR and luminescence) of new terbium and europium acylpyrazolonates, Inorganica Chim Acta 357 (2004) 4181–4190. https://doi.org/10.1016/j.ica.2004.06.024.

[9] X. Wu, S. Sun, J. Yang, Y. Wang, Y. Li, B. Su, Study of the Reaction Between the Nucleic Acid and Y-BPMPHD-CTMAB Complex and Its Analytical Application, J Fluoresc 14 (2004) 113–118. https://doi.org/10.1023/B:JOFL.0000014669.57732.89.

[10] Y. Jiang, S. Dey, H. Ke, Y. Yang, L. Sun, G. Xie, S. Chen, G. Rajaraman, Steric hindrance effect of Schiff-base ligands on magnetic relaxation dynamics and emissive behavior of two dinuclear dysprosium complexes, Journal of Rare Earths 41 (2023) 1049–1057. https://doi.org/10.1016/j.jre.2022.04.019.

[11] A. Hooda, D. Singh, K. Nehra, S. Dalal, V. Aggarwal, S. Kumar, R. Singh Malik, P. Kumar, Preparation and optical studies of octacoordinated luminescent complexes of Dy(III) derived from fluorinated β-diketone and heteroaromatic neutral ligands, Inorganica Chim Acta 556 (2023) 121674. https://doi.org/10.1016/j.ica.2023.121674.

[12] S. Dalal, D. Singh, A. Hooda, S. Redhu, S. Malik, V. Aggarwal, S. Kumar, R.S. Malik, P. Kumar, J. Sindhu, Enhancement in photophysical properties of octacoordinated Dy(III) complexes via energy transfer from photosensitizing ligands, Opt Mater (Amst) 150 (2024) 115159. https://doi.org/10.1016/j.optmat.2024.115159.

[13] S. Redhu, D. Singh, A. Hooda, A. Dalal, S. Kumar, R.S. Malik, V. Siwach, P. Kumar, Preparation, characterization and spectroscopic analyses of Dy(III) β-diketonates with bidentate N donor neutral ligands for displays, J Photochem Photobiol A Chem 449 (2024) 115381. https://doi.org/10.1016/j.jphotochem.2023.115381.

[14] M. Bedi, P. Chhillar, P. Dhankhar, J. Khanagwal, V.B. Taxak, S.P. Khatkar, P.B. Doon, New Insights into Optoelectronic Features of Eu(III) Complexes with Heterocyclic Ligand for Advanced Optical Applications, J Fluoresc 32 (2022) 1073–1087. https://doi.org/10.1007/s10895-022-02917-2.

[15] L. Reddy, A Review of the Efficiency of White Light (or Other) Emissions in Singly and Co-Doped Dy^{3+} Ions in Different Host (Phosphate, Silicate, Aluminate) Materials, J Fluoresc 33 (2023) 2181–2192. https://doi.org/10.1007/s10895-023-03250-y.

[16] H. Dalal, M. Kumar, S. Devi, P. Sehrawat, M. Sheoran, P. Devi, N. Sehrawat, R.K. Malik, Combustion Synthesis and Study of Double Charge Transfer in Highly Efficient Cool White-emitting Dy^{3+} Activated Vanadate-based Nanophosphor for Advanced Solid-state Lighting, J Fluoresc 33 (2023) 497–508. https://doi.org/10.1007/s10895-022-03098-8.

[17] G.M. Sheldrick, Crystal structure refinement with SHELXL, Acta Crystallogr C 71 (2015) 3–8. https://doi.org/10.1107/S2053229614024218.

[18] G.M. Sheldrick, SHELXT – Integrated space-group and crystal-structure determination, Acta Crystallogr A 71 (2015) 3–8. https://doi.org/10.1107/S2053273314026370.

[19] W.J. Geary, The use of conductivity measurements in organic solvents for the characterization of coordination compounds, Coord Chem Rev 7 (1971) 81–122. https://doi.org/10.1016/S0010-8545(00)80009-0.

[20] Y.A. Belousov, A.A. Drozdov, Lanthanide acylpyrazolonates: synthesis, properties and structural features, Russ Chem Rev 81 (2012) 1159. https://doi.org/10.1070/RC2012v081n12ABEH004255.

[21] Z.-F. Li, L. Zhou, J.-B. Yu, H.-J. Zhang, R.-P. Deng, Z.-P. Peng, Z.-Y. Guo, Synthesis, Structure, Photoluminescence, and Electroluminescence Properties of a New Dysprosium Complex, J Phys Chem C 111 (2007) 2295–2300. https://doi.org/10.1021/jp064749t.

[22] Z. Li, J. Yu, The near-infrared optical properties and Judd–Ofelt analysis of a Dy(III) complex, J Lumin 143 (2013) 169–172. https://doi.org/10.1016/j.jlumin.2013.04.044.

[23] K.Z. Wang, C.H. Huang, G.X. Xu, Y. Xu, Y.Q. Liu, D.B. Zhu, X.S. Zhao, X.M. Xie, N.Z. Wu, Preparation, Characterization, and Second-Harmonic Generation of a Langmuir-Blodgett Film Based on a Rare-Earth Coordination Compound, Mater Chem 6 (1994) 1986–1989. https://doi.org/10.1021/cm00047a017.

[24] F. Marchetti, R. Pettinari, C. Pettinari, Recent advances in acylpyrazolone metal complexes and their potential applications, Coord Chem Rev 303 (2015) 1–31. https://doi.org/10.1016/j.ccr.2015.05.003.

[25] V.F. Shul'gin, S. V Abkhairova, O. V Konnik, S.B. Meshkova, Z.M. Topilova, E.B. Rusanov, G.G. Aleksandrov, I.L. Eremenko, Anionic lanthanide complexes with 3-methyl-4-formyl-1-phenyl-5-pyrazolone, Russ J Inorg Chem 58 (2013) 678–683. https://doi.org/10.1134/S0036023613060223.

[26] Dejian Zhou, Qin Li, Chunhui Huang, Guangqing Yao, S. Umetani, M. Matsui, Liming Ying, Anchi Yu, Xinsheng Zhao, Room-temperature fluorescence, phosphorescence

and crystal structures of 4-acyl pyrazolone lanthanide complexes: $Ln(L)_3 \cdot 2H_2O$, Polyhedron 16 (1997) 1381–1389. https://doi.org/10.1016/S0277-5387(96)00382-8.

[27] Q. Liu, S. Zhang, K. Du, W. Li, Q. Yin, P. Cai, Structure and photoluminescence properties study of neodymium complexes containing fluorine ligands, J Fluor Chem 212 (2018) 161–165. https://doi.org/10.1016/j.jfluchem.2018.03.015.

[28] W. and M.J. and S.S. and S.M. and Z.C. Keese R. and Luef, Planarizing Distortions in Polycyclic Carbon Compounds, in: S. de Meijere Armin and Blechert (Ed.), Strain and Its Implications in Organic Chemistry: Organic Stress and Reactivity, Springer Netherlands, Dordrecht, 273 (1989) 283–296. https://doi.org/10.1007/978-94-009-0929-8_20.

[29] H. Debecca Devi, Ch. Sumitra, Th. David Singh, N. Yaiphaba, N. Mohondas Singh, N. Rajmuhon Singh, Calculation and Comparison of Energy Interaction and Intensity Parameters for the Interaction of Nd(III) with DL-Valine, DL-Alanine and β-Alanine in Presence and Absence of Ca^{2+}/Zn^{2+} in Aqueous and Different Aquated Organic Solvents Using 4f-4f Transition Spectra as Probe, Int J Spectrosc 2009 (2009) 1–9. https://doi.org/10.1155/2009/784305.

[30] R. Ilmi, K. Iftikhar, Pyrazine bridged Ln_2 (La, Nd, Eu and Tb) complexes containing fluorinated β-diketone, Inorg Chem Commun 20 (2012) 7–12. https://doi.org/10.1016/j.inoche.2012.01.037.

[31] M. Shoaib, R. Rajaramakrishna, G. Rooh, N. Chanthima, H.J. Kim, C. Saiyasombat, R. Botta, N. Nuntawong, S. Kothan, J. Kaewkhao, Structural and luminescence study of Dy^{3+} doped phosphate glasses for solid state lighting applications, Opt Mater (Amst) 109 (2020) 110322. https://doi.org/10.1016/j.optmat.2020.110322.

[32] E. Kaewnuam, N. Wantana, H.J. Kim, J. Kaewkhao, Development of lithium yttrium borate glass doped with Dy^{3+} for laser medium, W-LEDs and scintillation materials applications, J Non Cryst Solids 464 (2017) 96–103. https://doi.org/10.1016/j.jnoncrysol.2017.03.027.

[33] B. Liu, J. Shi, Q. Wang, H. Tang, J. Liu, H. Zhao, D. Li, J. Liu, X. Xu, Z. Wang, J. Xu, Crystal growth and yellow emission of Dy:$YAlO_3$, Opt Mater (Amst) 72 (2017) 208–213. https://doi.org/10.1016/j.optmat.2017.06.005.

[34] A. Ichoja, S. Hashim, S.K. Ghoshal, I.H. Hashim, Absorption and luminescence spectral analysis of Dy^{3+}-doped magnesium borate glass, Chin J Phys 66 (2020) 307–317. https://doi.org/10.1016/j.cjph.2020.03.029.

[35] S. Hussain, S. Ahmad, S. Sharif, S.S. Alarfaji, W.T.A. Harrison, X. Chen, Syntheses and crystal structures of lutetium(III) and dysprosium(III) coordination polymers with 2,5-dihydroxybenzene-1,4-dicarboxylate anion: Magnetic and photoluminescent properties of the dysprosium complex, Polyhedron 189 (2020) 114732. https://doi.org/10.1016/j.poly.2020.114732.

[36] R. Li, Y. Zhang, X. Liu, X. Chang, X. Feng, The synthesis, structural elucidation and fluorescent sensitization detection to Hg^{2+} based on two lanthanide-organic complexes, Inorganica Chim Acta 502 (2020) 119370. https://doi.org/10.1016/j.ica.2019.119370.

[37] N. Sabbatini, M. Guardigli, J.-M. Lehn, Luminescent lanthanide complexes as photochemical supramolecular devices, Coord Chem Rev 123 (1993) 201–228. https://doi.org/10.1016/0010-8545(93)85056-A.

Published Paper:

Polyhedron 247 (2024) 116701

Contents lists available at ScienceDirect

Polyhedron

journal homepage: www.elsevier.com/locate/poly

Fluorescent and electronic properties of Dysprosium acylpyrazolone complexes along with their synthesis and structural features

Maitrey Travadi [a], Rajendrasinh N. Jadeja [a,*], Ray J. Butcher [b]

[a] Department of Chemistry, Faculty of Science, The Maharaja Sayajirao University of Baroda, Vadodara 390002, India
[b] Department of Inorganic & Structural Chemistry, Howard University, Washington, DC 22031, USA

ARTICLE INFO

Keywords:
Dysprosium acylpyrazolone complexes
Distorted square antiprismatic geometry
Solid-state emission
Y/B ratio
Antenna energy diagram

ABSTRACT

Six distorted square antiprismatic eight coordinated Dysprosium acylpyrazolone complexes were synthesized having the compositions $[Dy(L_1)_3(EtOH)(H_2O)]$ (**DyL$_1$**), $[Dy(L_2)_3(EtOH)(H_2O)]$ (**DyL$_2$**), $[Dy(L_3)_3(EtOH)(H_2O)]$ (**DyL$_3$**), $[Dy(L_4)_3(EtOH)(H_2O)]$ (**DyL$_4$**), $[Dy(L_5)_3(EtOH)(H_2O)]$ (**DyL$_5$**), and $[Dy(L_6)_3(H_2O)(EtOH)]$ (**DyL$_6$**). The structure of all six complexes was examined using ESI-mass, FT-IR, UV–Vis, powder XRD, and thermogravimetric methods. According to the single crystal analysis of DyL_{4A}, the complex was found eight coordinated (DyO8) with a distorted square antiprismatic geometry. The comparison of stimulated powder pattern of DyL_{4A} crystal and experimental powder x-ray data helps to confirm the geometry of other complexes. In the solid-state emission spectra, the transition $^4F_{9/2}\rightarrow{}^6H_{13/2}$, which is close to the yellow region of the visible spectrum (~510–530 nm), exhibits hypersensitivity. The variance in intensity between electric-dipole and magnetic-dipole transition suggests a less asymmetric environment. The solvent effect has been thoroughly investigated through a comparative analysis of electronic spectra in different solvents. The intensity of emission spectra, Y/B ratio, and antenna effect energy diagram were examined from solid-state emission spectra.

1. Introduction

The coordination chemistry of lanthanide ions has attracted a lot of interest over the past two decades due to their advantageous magnetic, thermal, cytotoxic, redox, and optical properties, as well as their enormous coordination numbers, which enable highly complex and dimensional networks to be produced [1–6]. These lanthanide ions have a low level of absorbance and produce weak luminescence because 4f-4f transitions are prohibited. In these circumstances, it is desirable to use organic ligands, particularly β-diketones, as they have a high molar absorption coefficient and can coordinate and sensitise the Ln(III) ion through an indirect sensitization process known as the "antenna effect" [7]. Acylpyrazolone is an exclusive kind of β-diketones that has drawn more attention because of their variable 7 to 9 coordinated geometry, acute and high absorption coefficient values, proficient Antenna effect, luminous probe activities, catalytic and biological recognition activities [8–10]. The chemistry of acylpyrazolone complexes has drawn much interest because of their enormous potential for bio-enzymatic, electrical, photochromic, fluorescence probe, and catalytic activities [8–10].

The fluorescence characteristics of these derivatives have drawn more interest in recent years to the topic of lanthanide acylpyrazolone coordination chemistry [9]. Complexes of coumarin analogues of lanthanide ions were shown to have beneficial biological and pharmaceutical properties [11]. Complexes of pyrazoline and pyridine analogues of lanthanides are known for luminescent, optical, magnetic and metamaterial behaviour [12–14]. An ionic derivative of acylpyrazolones, $(Me_3NC_{16}H_{33})$ $[Al(Q_4Q)_2]$, first revealed their fluorescence activity [15]. Most frequently, low-intensity fluorescence and phosphorescence spectra were seen in terbium and europium complexes with the general formula $[M(Q)_3(H_2O)_2]$, $[M(Q)_3(EtOH)]$, or $[M(Q)_4]$, which have been associated to the auxiliary donors and substituents in acylpyrazolone ligands [16–18]. The line emission is visible in the fluorescence spectra of lanthanide acylpyrazolones because it results from environment-independent inner-shell electronic transitions at specific wavelengths [19]. Tridentate acylpyrazolone, which serves as a bridge ligand in binuclear complexes, has similar fluorescence spectra [20]. In the $(Me_3NC_{16}H_{33})[Ln(Q_3Q)_2]$ system, particularly with Sm^{3+}, Lu^{3+}, Y^{3+}, Gd^{3+} and Tb^{3+}, a good fluorescence enhancement effect with high intensity has been reported [21,22]. The approach for identifying nucleic acids is improved by the fluorescence quenching caused by nucleic acid in such a system [23].

Most lanthanide ions can display fluorescence, in which Dy^{3+}

* Corresponding author.
E-mail address: rjadeja-chem@msubaroda.ac.in (R.N. Jadeja).

https://doi.org/10.1016/j.poly.2023.116701
Received 6 September 2023; Accepted 21 October 2023
Available online 24 October 2023